Theor Chem Account (2009) 122:1–22
DOI 10.1007/s00214-008-0478-8

REGULAR ARTICLE

Thermodynamics of the gas-phase reactions in chemical vapor deposition of silicon carbide with methyltrichlorosilane precursor

Juanli Deng · Kehe Su · Xin Wang · Qingfeng Zeng · Laifei Cheng · Yongdong Xu · Litong Zhang

Received: 21 June 2008 / Accepted: 28 August 2008 / Published online: 23 September 2008

Abstract The gas-phase reaction thermodynamics in the chemical vapor deposition system of preparing silicon carbide via methyltrichlorosilane pyrolysis is investigated with a relatively complete set of 226 species, in which the thermodynamic data of 163 species are evaluated in this work with accurate model chemistry G3(MP2) and G3//B3LYP calculations combined with standard statistical thermodynamics. The data include heat capacity ($C^{\theta}_{p,\mathrm{m}}$), entropy ($S^{\theta}_{\mathrm{m}}$), enthalpy of formation ($\Delta_{\mathrm{f}}H^{\theta}_{\mathrm{m}}$) and Gibbs free energy of formation ($\Delta_{\mathrm{f}}G^{\theta}_{\mathrm{m}}$). All the results are consistent with the available reliable experiments. Based on these thermodynamic data, the equilibrium concentration distribution of the 226 possible species in 300–2,000 K is evaluated with the chemical equilibrium principle under a typical experimental condition. It is shown that the theoretical results are in very good agreement with the experiments. We conclude that the present work is instructive for experiments with different conditions.

Keywords Chemical vapor deposition · Equilibrium concentration distribution · Methyltrichlorosilane pyrolysis · Silicon carbide · Thermodynamics

1 Introduction

Silicon carbide (SiC), owing to its excellent physical and chemical stability, high thermal conductivity, strength and thermal shock resistance [1–3], has been widely studied experimentally [4–20] and theoretically [17–32]. The material has been successfully applied either as a functional or as a structural material, especially in the extreme environments (e.g., corrosive, high temperature and radiation in the fields of space vehicles, power, propulsion systems, turbine and piston engines, combustor liners, heat exchanger tubes and ceramic filters) [6, 7]. Among the different synthesis techniques [33–39], chemical vapor deposition (CVD) or chemical vapor infiltration (CVI) is the most advantageous method in the preparation of the structural materials. This is due to the considerable flexibility with respect to the fibers and matrices and the capacities to deposit high dense and pure matrix materials [9, 39]. This method is able to incorporate the reinforcing ceramic fibers in the ceramic matrix without chemically, mechanically or thermally damaging even with temperature and pressure variations [27]. The most frequently adopted precursor in the deposition is methyltrichlorosilane (CH_3SiCl_3 or MTS) [4–12, 14–20, 26–32] benefited from the equivalent ratio of silicon to carbon.

In understanding the CVD or CVI process in detail, the possibility of the complicated gas-phase chemistry reactions needs to be examined first with thermodynamics

Electronic supplementary material The online version of this article (doi:10.1007/s00214-008-0478-8) contains supplementary material, which is available to authorized users.

J. Deng · K. Su (✉) · X. Wang
School of Natural and Applied Sciences,
Northwestern Polytechnical University,
Xi'an, Shaanxi 710072, People's Republic of China
e-mail: sukehe@nwpu.edu.cn

Q. Zeng · L. Cheng · Y. Xu · L. Zhang
National Key Laboratory of Thermostructure Composite Materials, Northwestern Polytechnical University,
Xi'an, Shaanxi 710072, People's Republic of China

[17, 18, 20, 26, 27, 31, 40]. Thermodynamics is also able to indicate the formation of the condensed phases in different operating conditions and predict the optimized conditions. For this purpose, a relatively complete set of thermodynamic data for all the possible species is desirable. The data for most of the stable species can be found in the data sources such as the JANAF thermochemical tables [41], the thermodynamic properties of individual substances [42] or the NBS tables of chemical thermodynamic properties [43]. Those include the experimentally observed species (i.e., MTS, HCl, $SiCl_4$, CH_4, $HSiCl_3$, CH_3, CH_3Cl, Cl_2, C_2H_4, $SiCl_2$, $(SiCl_3)_{n=1,2}$, SiH_nCl_{6-n} and some of the SiC-clusters in Refs. [8, 9, 11, 20]) with Fourier transform infrared spectrometry [8, 9] or coherent anti-Stokes Raman spectroscopy [11] or the online gas chromatography [20]. A number of thermodynamic studies [17, 18, 20, 27] on the gas-phase composition have employed these data [41–43]. However, a large number of the short-lived radicals or highly reactive intermediates may also play important roles in the reactions, and most of them cannot be found in the tables [41–43]. Since the experimental detection is quite difficult [40], theoretical study thus becomes an alternative important means in developing the unknown data. For example, Papasouliotis et al. [10, 12, 14, 15, 27], Hüttinger [13], Allendorf et al. [21, 23, 26, 40] and Ge et al. [31, 32] performed very instructive investigations using the estimated thermodynamic data with the high accurate methods (i.e., bond additivity correction in Ref. [26] and effective CCSD(T)/aug-cc-pVTZ in Ref. [31]). However, the species involved in these studies could not be sufficient (e.g., 66, 77 and 50 species were considered in Refs. [26, 27, 31], respectively).

This work will consider a total number of 226 (221 gas phase and 5 condensed phase) species. The species are chosen from all of the possible dissociated stable intermediates, radicals and the associated species that may be formed by Si- and C-containing radicals. The associated hydrocarbons (or hydrosilicons) as well as their chlorides that have more than two carbon (or silicon) atoms are not considered in this work, because their number would be infinite. Since silicon carbides might be important in the nucleation or deposition, the C–Si clusters up to six heavy atoms will be included (like the C_{1-4} and Si_{1-4} clusters). The species that have the lowest energy (and the energy is close to the ground state) with different spin from the ground state will also be involved. Among the 221 gas-phase molecules, the thermochemistry data for 58 species are from our previous work (i.e., 5 gaseous atoms [41], 16 hydrocarbons [44], 2 SiC (in $X^1\Sigma$ and $a^3\Pi$ states) [45], 14 Si_mC_n ($3 \leq m + n \leq 6$) clusters [46] and 21 chlorohydrocarbons [47]). This work will focus on the remaining 163 species.

2 Calculation methods

2.1 Description of computational methods

Density functional theory (DFT) at B3PW91/6-31G(d) level is firstly used to optimize the geometries of 163 species. This method is chosen since it has been proven to reproduce the molecular geometries systematically better than a number of other methods [48], and its frequency scaling factor is established [49, 50]. Frequency analyses are performed following each optimization to confirm the stationary structure and to obtain the vibrational frequencies. Most of the low-lying electronic excitation (vertical excitations) energies are obtained with the time-dependent density functional theory (TD-DFT) [51] at B3PW91/6-31G(d) level. For a few species [SiCl–CH (C_s,$^1A'$), SiCl–CCl (C_s,$^1A'$) and C_4(D_{2h},^1A_g)] in which the TD-DFT misassigned the ground state as an excited state, additional second-order configuration interaction (SOCI) is employed to evaluate the electronic excitation energies. The reference states are chosen from the complete active space self-consistent field (CASSCF) calculations (using the GAMMESS program [52]). The multireference configuration interactions with singlet and doublet excitation (MR-CISD) calculations are carried out with the Xi'an-CI program based on the graphic unitary group approaches [53–57]. The geometries, vibrational frequencies and the electronic excitation energies are used in the standard statistical thermodynamic evaluations of the heat capacities and entropies of the species. The electronic energies are calculated with the accurate model chemistry G3(MP2) [58] and G3//B3LYP [59], since they have been examined to have average absolute deviations from the accurate experiments of the 299 reaction energies in the G2/97 test set [60, 61] by 1.30 and 0.99 kcal/mol, respectively. It is well known that those methods have been employed in the assessment of experiments or prediction of unknown thermochemistry data [62–64]. Most of the calculations are performed using the GAUSSIAN-03 program [65].

2.2 Heat capacity and entropy

Heat capacities ($C^{\theta}_{p,\mathrm{m}}$) and entropies ($S^{\theta}_{\mathrm{m}}$) at different temperatures are evaluated with the standard statistical thermodynamics procedures. The frequencies used in the vibrational partition functions are scaled with the factors from Ref. [49], i.e., 0.9573 for fundamental frequency, 0.9885 for heat capacity and 0.9920 for entropy. The electronic excitations calculated with TD-DFT at B3PW91/6-31G(d) level are truncated at 15,000 cm^{-1} or at 1.860 eV, which has been proven to be sufficient for electronic contributions to heat capacity and entropy of a

molecule at temperature as high as 2,000 K [45]. The anharmonic corrections are neglected as has been discussed in Ref. [45]. The heat capacity ($C^{\theta}_{p,\mathrm{m}}$) and entropy ($S^{\theta}_{\mathrm{m}}$) are formulated in Eqs. 1–4.

For linear molecules,

$$C^{\theta}_{p,\mathrm{m}}(T) = R\left\{\frac{7}{2} + \sum_{i=1}^{3n-5}\left[e^{hv_i/kT}\left(\frac{hv_i/kT}{e^{hv_i/kT}-1}\right)^2\right] + \frac{\sum_i g_i\varepsilon_i^2 e^{-\varepsilon_i/kT}\sum_i g_i e^{-\varepsilon_i/kT} - \left(\sum_i g_i\varepsilon_i e^{-\varepsilon_i/kT}\right)^2}{\left(kT\sum_i g_i e^{-\varepsilon_i/kT}\right)^2}\right\} \quad (1)$$

$$S^{\theta}_{\mathrm{m}}(T) = R\left\{\begin{array}{l} \frac{7}{2} + \ln\left[\left(\frac{2\pi mkT}{h^2}\right)^{3/2}\frac{kT}{p^{\theta}}\right] + \ln\left(\frac{8\pi^2 IkT}{\sigma h^2}\right) \\ + \sum_{i=1}^{3n-5}\left[\frac{hv_i/kT}{e^{hv_i/kT}-1} - \ln\left(1-e^{-hv_i/kT}\right)\right] \\ + \ln\left(\sum_i g_i e^{-\varepsilon_i/kT}\right) + \frac{1}{kT}\frac{\sum_i g_i\varepsilon_i e^{-\varepsilon_i/kT}}{\sum_i g_i e^{-\varepsilon_i/kT}} \end{array}\right\} \quad (2)$$

For nonlinear molecules,

$$C^{\theta}_{p,\mathrm{m}}(T) = R\left\{4 + \sum_{i=1}^{3n-6}\left[e^{hv_i/kT}\left(\frac{hv_i/kT}{e^{hv_i/kT}-1}\right)^2\right] + \frac{\sum_i g_i\varepsilon_i^2 e^{-\varepsilon_i/kT}\sum_i g_i e^{-\varepsilon_i/kT} - \left(\sum_i g_i\varepsilon_i e^{-\varepsilon_i/kT}\right)^2}{\left(kT\sum_i g_i e^{-\varepsilon_i/kT}\right)^2}\right\} \quad (3)$$

$$S^{\theta}_{\mathrm{m}}(T) = R\left\{\begin{array}{l} 4 + \ln\left[\left(\frac{2\pi mkT}{h^2}\right)^{3/2}\frac{kT}{p^{\theta}}\right] \\ + \ln\left(\frac{8\pi^2(2\pi kT)^{3/2}}{\sigma h^3}\left(I_xI_yI_z\right)^{1/2}\right) \\ + \sum_{i=1}^{3n-6}\left[\frac{hv_i/kT}{e^{hv_i/kT}-1} - \ln\left(1-e^{-hv_i/kT}\right)\right] \\ + \ln\left(\sum_i g_i e^{-\varepsilon_i/kT}\right) + \frac{1}{kT}\frac{\sum_i g_i\varepsilon_i e^{-\varepsilon_i/kT}}{\sum_i g_i e^{-\varepsilon_i/kT}} \end{array}\right\} \quad (4)$$

where R is the molar gas constant, n is the number of atoms in the system, h is the Planck's constant, v_i is the vibrational frequency of the ith mode, k is the Boltzmann constant, g_i is the quantum weight (degeneracy) of the ith electronic energy state, ε_i is the energy of the ith state, σ is the symmetry number and I is the moment of inertia of the molecule.

To simplify the applications of the high-temperature thermodynamic data, polynomial fitting of the theoretical heat capacities obtained via Eq. 1 or Eq. 3 is carried out. The polynomial equation is in the form of Ref. [66] as shown in Eq. 5.

$$C^{\theta}_{\mathrm{p},m}(T) = a_0 + a_1T + a_2T^2 + a_3T^3 + a_4T^{-2} \quad (5)$$

2.3 Enthalpy and Gibbs free energy of formation

Enthalpy of formation $\Delta_{\mathrm{f}}H^{\theta}_{\mathrm{m}}$ and Gibbs free energy of formation $\Delta_{\mathrm{f}}G^{\theta}_{\mathrm{m}}$ are predicted with the atomization reaction as shown in Eq. 6. The calculation details are

$$\mathrm{Si}_m\mathrm{C}_n\mathrm{H}_x\mathrm{Cl}_y(\mathrm{gas}) \rightarrow m\mathrm{Si}(\mathrm{gas}) + n\mathrm{C}(\mathrm{gas}) + x\mathrm{H}(\mathrm{gas}) + y\mathrm{Cl}(\mathrm{gas}) \quad (6)$$

$$\Delta_{\mathrm{f}}H^{\theta}_{\mathrm{m}}(\mathrm{Si}_m\mathrm{C}_n\mathrm{H}_x\mathrm{Cl}_y, g, T) = \sum_i^{\mathrm{atoms}}\mu_i\Delta_{\mathrm{f}}H^{\theta}_{\mathrm{m}}(i, g, T) - \Delta_{\mathrm{r}}H^{\theta}_{\mathrm{m}}(T) \quad (7)$$

$$\Delta_{\mathrm{f}}G^{\theta}_{\mathrm{m}}(\mathrm{Si}_m\mathrm{C}_n\mathrm{H}_x\mathrm{Cl}_y, g, T) = \sum_i^{\mathrm{atoms}}\mu_i\Delta_{\mathrm{f}}G^{\theta}_{\mathrm{m}}(i, g, T) - \Delta_{\mathrm{r}}G^{\theta}_{\mathrm{m}}(T) \quad (8)$$

where, μ_i is the chemometrics number of species i, $\Delta_{\mathrm{f}}H^{\theta}_{\mathrm{m}}(i,\mathrm{g},T)$ and $\Delta_{\mathrm{f}}G^{\theta}_{\mathrm{m}}(i,\mathrm{g},T)$ of atom i are the experimental data, which can be found, for example, from JANAF [41] or CODATA [67]. $\Delta_{\mathrm{r}}H^{\theta}_{\mathrm{m}}(T)$ and $\Delta_{\mathrm{r}}G^{\theta}_{\mathrm{m}}(T)$ in Eqs. 7 and 8 are the enthalpy and Gibbs free energy changes of the reaction obtained with Eqs. 9 and 10.

$$\Delta_{\mathrm{r}}H^{\theta}_{\mathrm{m}}(T) = \sum_i \mu_i H^{\theta}_{\mathrm{m}}(298.15\ \mathrm{K}) + \int_{298.15}^{T}\sum_i \mu_i C^{\theta}_{p,\mathrm{m}}(T)\mathrm{d}T \quad (9)$$

$$\Delta_{\mathrm{r}}G^{\theta}_{\mathrm{m}}(T) = \Delta_{\mathrm{r}}H^{\theta}_{\mathrm{m}}(T) - T\left[\sum_i \mu_i S^{\theta}_{\mathrm{m}}(298.15\ \mathrm{K}) + \int_{298.15}^{T}\frac{\sum_i \mu_i C^{\theta}_{p,\mathrm{m}}(T)}{T}\mathrm{d}T\right] \quad (10)$$

where $H^{\theta}_{\mathrm{m}}(298.15\ \mathrm{K})$ is the standard enthalpy at 298.15 K obtained by G3(MP2) or G3//B3LYP electronic energy combined with statistical thermodynamics, $C^{\theta}_{p,\mathrm{m}}(T)$ is the standard molar heat capacity of Eq. 5 fitted with the data of Eq. 1 for linear and of Eq. 3 for nonlinear molecules and $S^{\theta}_{\mathrm{m}}(298.15\ \mathrm{K})$ is the standard entropy at 298.15 K obtained with Eq. 2 for linear and with Eq. 4 for nonlinear molecules.

To assess the reliability of the theoretical predictions, especially at higher temperatures, the results for the species, which have well-established experimental or theoretical data, will be compared with the fourth edition of the *NIST-JANAF thermochemical tables* [41], *Thermodynamic properties of individual substances* [42] and others [66–69].

2.4 Gas-phase equilibrium calculation

Equilibrium distribution of the species involved in this work as a function of temperature can be obtained according to the principle of chemical equilibrium by minimizing the total partial molar Gibbs free energy (or the total chemical potential) of the system as shown in Eq. 11.

$$\min G = \min\left\{\sum_{i=1}^{s} n_i^{\mathrm{cond}} \Delta G^{\theta}_{\mathrm{m},i}(\mathrm{cond.}) + \sum_{i=s+1}^{N} n_i \left[\Delta G^{\theta}_{\mathrm{m},i}(\mathrm{gas}) + RT\ln p + RT\ln\frac{n_i}{\sum_{j=s+1}^{N} n_j}\right]\right\} \tag{11}$$

where s is the total number of the condensed-phase species, N is total number of the species in the system (consequently the number of gaseous species is $N-s$), p is the total pressure, n_i is the number of moles of the ith gaseous species and n_i^{cond} is the number of moles of the ith condensed-phase species satisfying

$$\sum_{i=1}^{N} a_{ij} n_i = B_j \quad (j = 1, 2, \ldots, M)$$

where a_{ij} is the atomicity of element j in species i, B_j is the total atomicity of element j and M is the total number of different elements.

In Eq. 11, the standard molar Gibbs free energy either for condensed-phase $\Delta G^{\theta}_{\mathrm{m}}(\mathrm{cond.})$ or for gaseous species $\Delta G^{\theta}_{\mathrm{m}}(\mathrm{gas})$ at any temperature T is defined as

$$\Delta G^{\theta}_{\mathrm{m}}(T) = \Delta H^{\theta}_{\mathrm{m}}(T) - T\Delta S^{\theta}_{\mathrm{m}}(T)$$

in which

$$\Delta H^{\theta}_{\mathrm{m}}(T) = \Delta_{\mathrm{f}} H^{\theta}_{\mathrm{m}}(298.15\ \mathrm{K}) + \int_{298.15}^{T} C_{p,\mathrm{m}}\mathrm{d}T$$

and

$$\Delta S^{\theta}_{\mathrm{m}}(T) = S^{\theta}_{\mathrm{m}}(298.15\ \mathrm{K}) + \int_{298.15}^{T} \frac{C_{p,\mathrm{m}}}{T}\mathrm{d}T$$

The gas-phase diagrams are obtained with a code [70] developed in our group.

3 Results and discussion

3.1 Structure, vibrational frequency and electronic excitation energy

Structure The structure, symmetry and electronic state of the 163 species in the MTS pyrolysis system obtained with B3PW91/6-31G(d) calculations are shown in Fig. 1.

Compared with some of the experimental available species [i.e., SiH_3Cl(No. 126), $SiCl_3H$(127), SiH_2Cl_2(128), SiHCl(130), SiH(134), SiH_2(135), SiH_3(137), SiH_4(138), SiCl(145), $SiCl_2$(146), $SiCl_3$(148), $SiCl_4$(149), Si_2(156) and Si_3(158) in Ref. [41]), the predicted stable structure, symmetry and electronic state are the same. Only Si_3(158) molecule is an exception. The present calculations resulted $Si_3(^1A_1)$ in a triangular C_{2v} geometry, while Ref. [41] estimated a linear. The linear structure was found in the present work to be an unstable molecule with two imaginary vibrational frequencies. Only the triangle will be considered. The triangle geometry is consistent with the structure proposed in Ref. [42] obtained theoretically from Refs. [71–74].

Vibrational frequency The fundamental vibrational frequencies (scaled by 0.9573 [49]) and the respective infrared spectra intensities obtained with B3PW91/6-31G(d) are listed in Supplement Material 1. The frequency analyses have confirmed that all the 163 species are stationary structures (without imaginary frequency). Compared with the values of the experimental available species [i.e., SiH_3Cl(126), $SiCl_3H$(127), SiH_2Cl_2(128), SiHCl(130), SiH(134), SiH_2(135), SiH_3(137), SiH_4(138), SiCl(145), $SiCl_2$(146), $SiCl_3$(148), $SiCl_4$(149) and Si_2(156) in Ref. [41]], the theoretical frequencies are consistent within $\pm 47\ \mathrm{cm}^{-1}$. The only exception is in SiH(134) radical, which has a slightly larger deviation of $-92\ \mathrm{cm}^{-1}$. But this is consistent with the result from a number of theoretical methods reported in Ref. [66] that the theoretical frequency is systematically smaller at the similar magnitude. Since the theoretical methods generally reproduce the experimental geometries and vibrational frequencies well, especially from DFT calculations [49], the frequencies calculated in this work are reasonably believed well.

Electronic excitation energy As has been examined [45], the electronic excitation energy is important in the statistical evaluation of the thermochemical data. However, the higher (>1.860 eV or 15,000 cm^{-1}) excitations will lead to negligible corrections to the heat capacity or entropy even at temperatures up to 2,000 K (i.e., the maximum contribution being 0.16 J K^{-1} mol^{-1} for $C_{p,\mathrm{m}}$ and 0.016 J K^{-1} mol^{-1} for S_{m} in a molecule if one excited state is involved [45]). This work will also consider the electronic excitation energies within the region of 1.860 eV. The results for the species having at least one electronic excitation energy inside the truncation region computed with TD-DFT B3PW91/6-31G(d) (and with SOCI in four cases where TD-DFT resulted in a negative excitation energy) are collected in Table 1.

Among all the 163 species, 72 are found to have the low-lying excited states in our truncation region

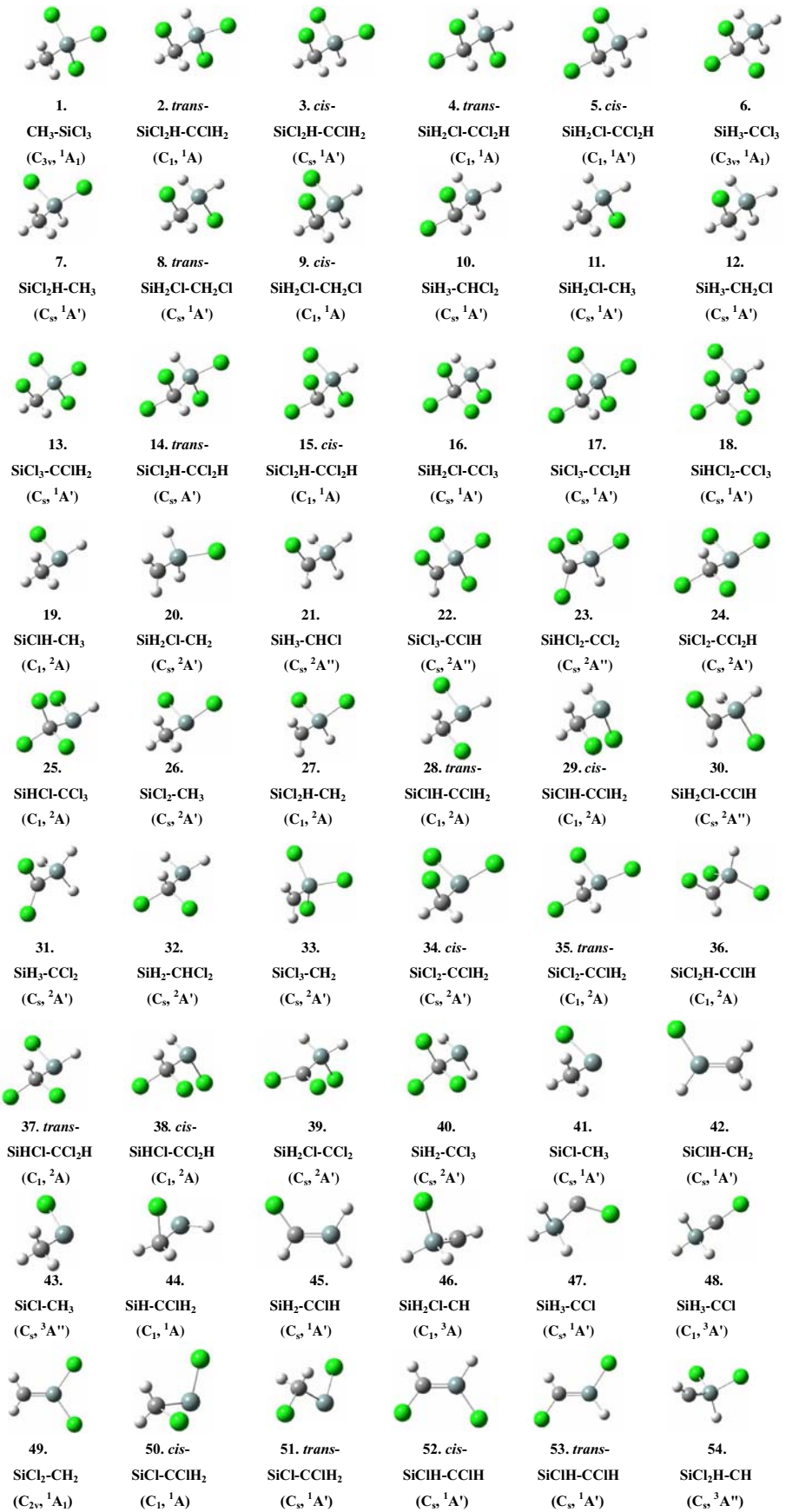

Fig. 1 Stable structure (symmetry and electronic state) of the 163 species in the MTS pyrolysis system obtained with B3PW91/6-31G(d) calculations. Numbering of the species will be kept the same in the tables, figures and in text of this paper

Fig. 1 continued

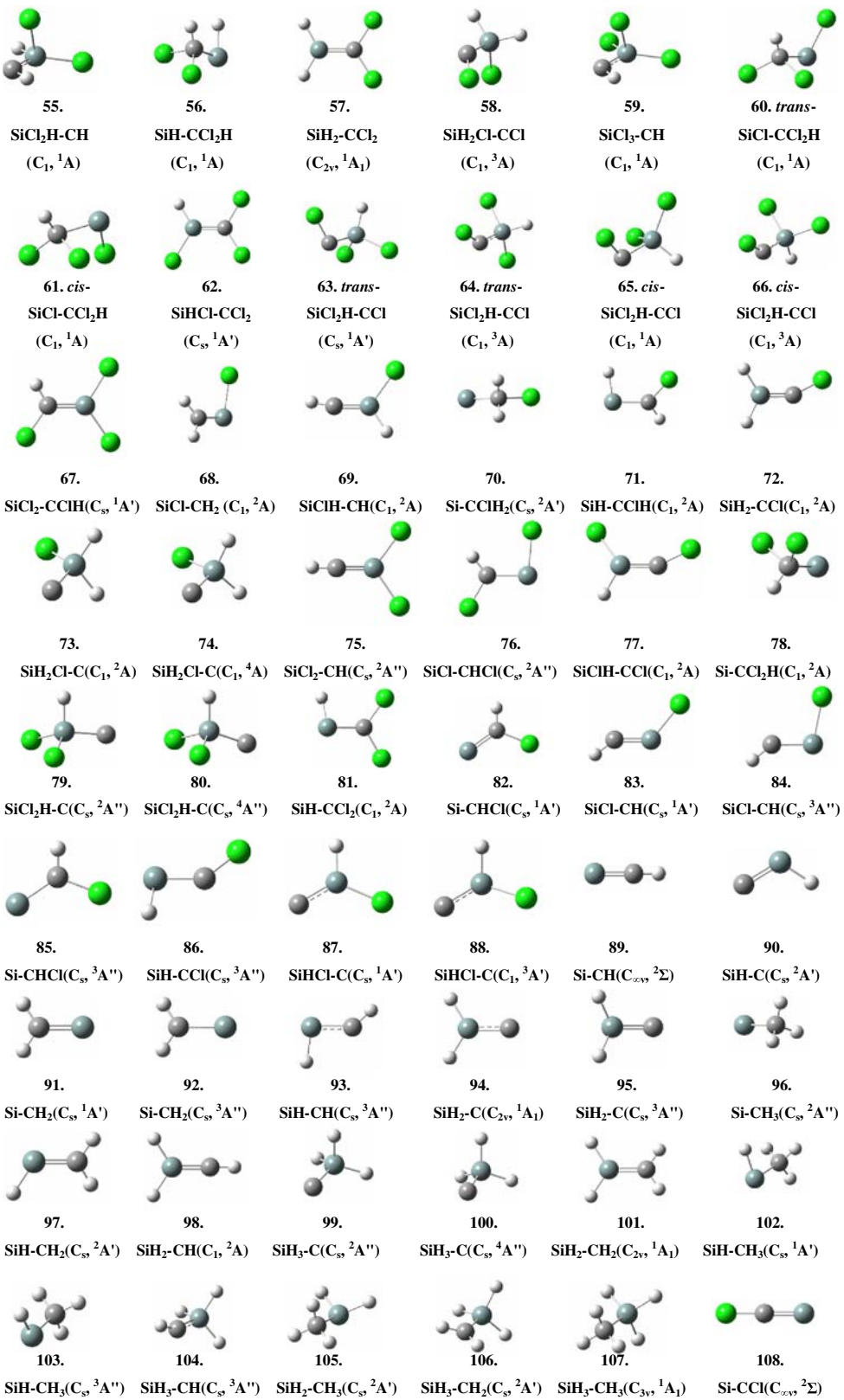

(≤1.860 eV) that will lead to considerable corrections to the high-temperature thermochemistry data. Compared with the available experiments [42, 73, 75] on the transitions of $Si_2(156)(X^3\Sigma_g \rightarrow A^3\Pi_u)$, $Si_3(158)(X^1A_1 \rightarrow a^3B_1$, $X^1A_1 \rightarrow b^3A_1$, $X^1A_1 \rightarrow c^3B_1$, $X^1A_1 \rightarrow A^1B_2$, $X^1A_1 \rightarrow B^1B_1$ and $X^1A_1 \rightarrow f^3B_2)$ and $Si_4(159)(X^1A_g \rightarrow$

Fig. 1 continued

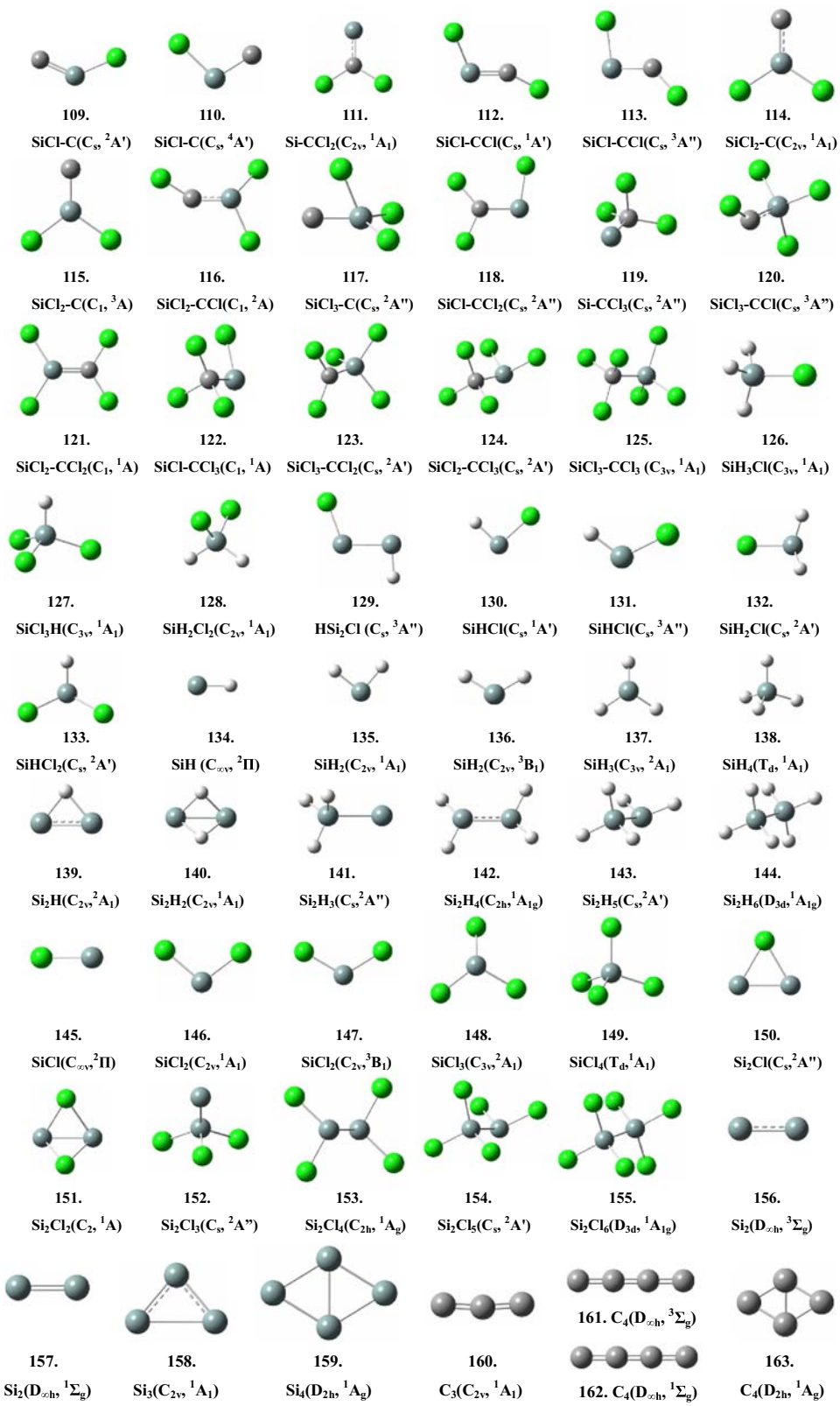

a^3B_{3u}, $X^1A_g \rightarrow A^1B_{3u}$, $X^1A_g \rightarrow c^3B_{1g}$ and $X^1A_g \rightarrow d^3B_{1u}$), most of the calculated results are in good agreements. The deviations are 0.112–0.123, −0.072, −0.221, −0.101, −0.130, 0.049, −0.138, 0.147, −0.119, −0.09 and 0.108 eV, respectively. The maximum deviation of 0.123 eV on Si_2(156) will lead to the heat capacity changes

Table 1 Low-lying (≤1.860 eV) vertical excitation energies calculated with TD-DFT at B3PW91/6-31G(d) level

No.[a]	Species (symmetry, state)	State	ε_i (eV)	g_i	No.[a]	Species(symmetry, state)	State	ε_i (eV)	g_i
41	SiCl–CH_3(C_s, $^1A'$)	a^3A''	1.294	3	110	SiCl–C(C_s, $^4A''$)	a^2A'	0.484	2
47	SiH_3–CCl(C_s, $^1A'$)	A^1A	0.879	1			b^2A''	0.827	2
48	SiH_3–CCl(C_1, ^3A)	a^1A	0.752	1			c^2A'	1.201	2
		b^1A	1.631	1			d^2A''	1.781	2
51	*trans*-SiCl–$CClH_2$(C_s, $^1A'$)	a^3A''	1.432	3	111	Si–CCl_2(C_{2v}, $^1A_1$)	a^3A_2	0.822	3
55	$SiCl_2H$–CH(C_1, ^1A)	a^3A	0.622	3			A^1A_2	1.357	1
57	SiH_2–CCl_2(C_{2v}, $^1A_1$)	a^3A_1	1.604	3			b^3A_1	1.760	3
59	$SiCl_3$–CH(C_1, ^1A)	a^3A	0.126	3	112	SiCl–CCl(C_s, $^1A'$)[d]	a^3A''	0.673	3
63	*trans*-$SiCl_2H$–CCl(C_s, $^1A'$)	A^1A''	0.882	1			b^3A'	1.429	3
65	*cis*-$SiCl_2H$–CCl(C_1, ^1A)	A^1A	0.811	1			A^1A''	1.517	1
66	*cis*-$SiCl_2H$–CCl(C_1, ^3A)	a^1A	0.705	1	113	SiCl–CCl(C_s, $^3A''$)	A^3A''	1.631	3
		b^1A	1.510	1	114	$SiCl_2$–C(C_{2v}, $^1A_1$)	A^1A_2	0.261	1
68	SiCl–CH_2(C_1, ^2A)	A^2A_1	1.052	2			B^1B_2	1.788	1
69	SiClH–CH(C_1, ^2A)	A^2A	1.289	2	115	$SiCl_2$–C(C_1, ^3A)	A^3A	1.271	3
70	Si–$CClH_2$(C_s, $^2A'$)	A^2A''	0.247	2	116	$SiCl_2$–CCl(C_1, ^2A)	A^2A	1.593	2
71	SiH–CClH(C_1, ^2A)	A^2A	1.230	2			B^2A	1.806	2
72	SiH_2–CCl(C_1, ^2A)	A^2A	1.637	2	117	$SiCl_3$–C(C_s, $^2A''$)	X^2A''	1.726	2
73	SiH_2Cl–C(C_1, ^2A)	A^2A	0.524	2			A^2A'	1.752	2
		A^2A	1.754	2	118	SiCl–CCl_2(C_s, $^2A''$)	A^2A''	1.430	2
74	SiH_2Cl–C(C_1, ^4A)	A^2A	0.962	2	119	Si–CCl_3(C_s, $^2A''$)	A^2A''	1.278	2
		A^2A	1.486	2	121	$SiCl_2$–CCl_2(C_1, ^1A)	A^3A	1.141	3
75	$SiCl_2$–CH(C_s, $^2A''$)	A^2A''	1.285	2	129	HSi_2Cl(C_s, $^3A''$)	A^3A''	1.729	3
76	SiCl–CHCl(C_s, $^2A''$)	A^2A''	1.226	2	130	SiHCl(C_s, $^1A'$)	a^3A''	1.178	3
77	SiClH–CCl(C_1, ^2A)	A^2A	1.261	2	134	SiH($C_{\infty v}$, $^2\Pi$)	$A^2\Sigma_g$	0.016	2[c]
78	Si–CCl_2H(C_1, ^2A)	A^2A	1.237	2				1.689	2
79	$SiCl_2H$–C(C_s, $^2A''$)	A^2A''	0.329	2	135	SiH_2(C_{2v}, $^1A_1$)	a^3B_1	0.520	3
		A^2A'	1.607	2	145	SiCl($C_{\infty v}$, $^2\Pi$)		0.012	2[c]
81	SiH–CCl_2(C_1, ^2A)	A^2A	1.276	2	150	Si_2Cl(C_s, $^2A''$)	A^2A''	0.779	2
82	Si–CHCl(C_s, $^1A'$)	a^3A''	1.038	3			B^2A''	1.695	2
		A^1A''	1.560	1	152	Si_2Cl_3(C_s, $^2A''$)	A^2A''	1.443	2
83	SiCl–CH(C_s, $^1A'$)[b]	a^3A''	1.209	3	153	Si_2Cl_4(C_{2h}, ^1A_g)	a^3B_u	0.101	3
		A^3A'	1.405	3	156	Si_2($D_{\infty h}$, $^3\Sigma_g$)	$A^3\Pi_u$	0.1369 (0.012–0.025)[e]	6
84	SiCl–CH(C_s, $^3A''$)	A^3A''	1.228	3			$a^1\Delta$	0.7319	2
85	Si–CHCl(C_s, $^3A''$)	A^3A''	1.145	3			$b^1\Sigma_g$	0.7510	1
		B^3A''	1.609	3			$c^1\Pi_u$	0.9939	2
86	SiH–CCl(C_s, $^3A''$)	A^3A''	1.185	3			$B^3\Pi_g$	1.7294	6
87	SiHCl–C(C_s, $^1A'$)	A^1A''	0.494	1	157	Si_2($D_{\infty h}$, $^1\Sigma_g$)	$a^3\Sigma_u$	1.070	3
		B^1A'	1.544	1	158	Si_3(C_{2v}, $^1A_1$)	a^3B_2	0.233 (0.161)[f]	3
88	SiHCl–C(C_1, ^3A)	A^3A''	0.473	3			b^3A_1	0.841 (0.620)[f]	3
89	Si–CH($C_{\infty v}$, $^2\Pi$)		0.014	2			c^3B_1	1.105 (1.004)[f]	3
90	SiH–C(C_s, $^2A'$)	A^2A''	0.352	2			A^1B_2	1.283 (1.153)[f]	1
		B^2A'	0.643	2			B^1B_1	1.637 (1.686)[f]	1
		B^2A''	1.103	2			d^3B_1	1.641	3
91	Si–CH_2(C_s, $^1A'$)	a^3A''	1.697	3			e^3B_2	1.861 (1.723)[f]	3
92	Si–CH_2(C_s, $^3A''$)	A^3A''	0.926	3	159	Si_4(D_{2h}, ^1A_g)	a^3B_{3u}	0.669 (0.816)[g]	3
		B^3A'	1.375	3			A^1B_{3u}	1.489 (1.370)[g]	1
93	SiH–CH(C_s, $^3A''$)	A^3A''	0.860	3			b^3B_{2g}	1.500	3
94	SiH_2–C(C_{2v}, $^1A_1$)	A^1A_2	0.863	1			B^1B_{2g}	1.586	1
		B^1B_2	1.566	1			c^3B_{1g}	1.801 (1.711)[g]	3
		a^3A_1	1.833	3			d^3B_{1u}	1.823 (1.931)[g]	3
95	SiH_2–C(C_s, $^3A''$)	A^3A'	0.952	3	160	C_3(C_{2v}, $^1A_1$)	a^3B_1	1.685	3
96	Si–CH_3(C_s, $^2A''$)	A^2A''	0.137	2			b^3A_1	1.696	3

Table 1 continued

No.[a]	Species (symmetry, state)	State	ε_i (eV)	g_i	No.[a]	Species(symmetry, state)	State	ε_i (eV)	g_i
97	SiH–CH_2(C_s, $^2A'$)	A^2A''	1.493	2	161	C_4($D_{\infty h}$, $^3\Sigma_g$)	$A^3\Pi_g$	1.203	6
98	SiH_2–CH(C_1, ^2A)	A^2A	1.812	2			$B^3\Pi_u$	1.509	6
99	SiH_3–C(C_s, $^2A''$)	A^2A''	0.486	2			$a^1\Pi_u$	1.693	2
100	SiH_3–C(C_s, $^4A''$)	a^2A''	0.939	2	162	C_4($D_{\infty h}$, $^1\Sigma_g$)	$A^1\Pi_g$	1.233	2
		b^2A''	1.424	2			$a^3\Sigma_u$	1.580	3
102	SiH–CH_3(C_s, $^1A'$)	a^3A''	0.633	3			$B^1\Sigma_u$	1.693	1
108	Si–CCl($C_{\infty v}$, $^2\Pi$)		0.010	2[c]	163	C_4(D_{2h}, ^1A_g)[h]	a^3B_{1u}	0.972	3
109	SiCl–C(C_s, $^2A'$)	A^2A''	0.343	2			b^3B_{2g}	1.825	3
		B^2A'	0.717	2					
		C^2A''	1.297	2					

[a] Numbering of the molecules is the same as in Fig. 1. The species without excitation energy in the truncation region (<1.860 eV or <15,000 cm^{-1}) are not listed in this table

[b] Excitation energy is calculated with second-order configuration interaction of singlet and doublet substitutions (SOCISD) combined with Davidson corrections (DC) of size-consistency [76, 77] [i.e., 12, 8 and 7 reference states (RS) from CASSCF(4,4)/6–31(d) are involved for SiCl–CH(X^1A'), SiCl–CH($^3A''$) and SiCl–CH($^3A'$), respectively. The respective number of configuration state functions (CSFs) is 2,403,637, 3,719,661 and 3,804,194]

[c] The electron is actually excited into the electronic degenerated state (i.e., the 'excited state' is a quasi-excited state with respect to the state from which the electron is excited). Therefore, the weight is half on either states

[d] CASSCF(4,4)/6–31G(d)-SOCISD + DC [RS = 12 and CSFs = 7,856,839 for SiCl–CCl(X^1A'), RS = 8 and CSFs = 12,202,873 for SiCl–CCl($^3A''$), RS = 8 and CSFs = 12,578,963 for SiCl–CCl($^3A'$) and RS = 8 and CSFs = 6,925,519 for SiCl–CCl($^1A''$)]

[e] Ref. [75]; [f] Ref. [42]; [g] Ref. [89]

[h] CASSCF(8,8)/6–31G(d)-SOCISD+DC [RS = 252 and CSFs = 12,094,080 for C_4(X^1A_g), RS = 296 and CSFs = 22,856,968 for C_4($^3B_{1u}$), RS = 296 and CSFs = 22857512 for C_4($^3B_{2g}$)]

at 298.15, 600 and 2,000 K by 1.77, 6.20 and 1.55 J K^{-1} mol^{-1}, respectively. The deviations on Si_3(158) will lead to the heat capacity changes at 298.15, 400 and 2,000 K by 1.59, 3.50 and −0.91 J K^{-1} mol^{-1} and those on Si_4(159) will lead to the same changes at 298.15 and 2,000 K by 0 and 2.11 J K^{-1} mol^{-1}, respectively. The largest deviation (6.20) corresponds to the error (6.20 × 600/1,000) of energy by 3.72 kJ mol^{-1}, which is less than 1 kcal/mol. Therefore, the electronic excitation energies calculated in this work are acceptable.

3.2 Heat capacity and entropy

By utilizing the structural parameters, vibrational frequencies and electronic excitation energies of 163 species, the standard molar heat capacity $C^{\theta}_{p,m}$ and entropy S^{θ}_{m} are developed via Eqs. 1–4. The results at 298.15 K for 17 species having experimental or theoretical data are listed in Table 2. The respective data from experiments and calculations [41, 42, 67, 68] are also listed for comparison.

As shown in Table 2, the calculated results are in excellent agreement with the available experiments [41, 42, 67, 68] except for Si_2(156) molecule. The mean absolute deviations are only 0.603, 0.376, 0.568 and 0.325 J mol^{-1} K^{-1} for $C^{\theta}_{p,m}$ (298.15 K) and 1.028, 0.707, 1.117 and 0.917 J mol^{-1} K^{-1} for S^{θ}_{m} (298.15 K) compared with Refs. [41], [42], [67] and [68], respectively. For Si_2(156), the larger deviation of $C^{\theta}_{p,m}$ (298.15 K) is 0.38 J mol^{-1} K^{-1} and that of S^{θ}_{m} (298.15 K) is −7.4 J mol^{-1} K^{-1} compared with Refs. [42, 67]. The deviation is mainly from the difference of electronic excitation energies and will be discussed later. It can thus be concluded that the present calculations are qualified to predict the thermodynamic data of the other species. The results are listed in Supplement Material 2.

Comparisons of the heat capacity $C^{\theta}_{p,m}$ and entropy S^{θ}_{m} obtained with Eqs. 1–4 within 100–2,000 K for the 14 experimental available species [SiH_3Cl(No. 126), $SiCl_3H$(127), SiH_2Cl_2(128), SiHCl(130), SiH(134), SiH_2(135), SiH_3(137), SiH_4(138), SiCl(145), $SiCl_2$(146), $SiCl_3$(148), $SiCl_4$(149), Si_2(156) and Si_3(158)] in Ref. [41] or [42] are shown in Fig. 2a–n.

As shown in the Fig. 2, the predicted heat capacities and entropies are also consistent with the experiments in Refs. [41, 42] even at high temperatures. Most of the curves [i.e., SiH_3Cl(No. 126), $SiCl_3H$(127), SiH_2Cl_2(128), SiHCl(130), SiH_2(135), SiH_3(137), SiH_4(138), $SiCl_2$(146), $SiCl_3$(148) and $SiCl_4$(149)] are in excellent agreement with the experiments within ±1.7 J mol^{-1} K^{-1} for heat capacities and within ±1.6 J mol^{-1} K^{-1} for entropies.

The heat capacities of SiH(134), SiCl(145), Si_2(156) and Si_3(158) have larger differences. In fact, the data of SiH(134) have the largest deviation only by −1.06 or −2.22 J mol^{-1} K^{-1} compared with Ref. [41] or [42], respectively, at the highest temperature of 2,000 K. The deviation of SiCl(145) is also within −1.74 J mol^{-1} K^{-1} compared with either Ref. [41] or Ref. [42]. The heat

Table 2 Comparison of the heat capacity $C^{\theta}_{p,m}$(298.15 K) and entropy S^{θ}_{m}(298.15 K) of the experimentally or theoretically available species

No.[a]	Species (symmetry, state)	$C^{\theta}_{p,m}$ (298.15 K) (J mol^{-1} K^{-1})		S^{θ}_{m} (298.15 K) (J mol^{-1} K^{-1})	
		Cal.	Ref.	Cal.	Ref.
1	CH_3–$SiCl_3$(C_{3v}, $^1A_1$)	104.016	102.382[b]	349.711	351.147[b]
					351.09[c]
107	SiH_3–CH_3(C_{3v}, $^1A_1$)	66.100	65.9[d]	255.917	256.5[d]
126	SiH_3Cl(C_{3v}, $^1A_1$)	51.511	51.098[b]	251.102	250.761 ± 0.21[b]
			51.08[c]		250.76[c]
			51.0[d]		250.7[d]
127	$SiCl_3H$(C_{3v}, $^1A_1$)	75.973	75.455[b]	314.898	313.717 ± 0.4[b]
			75.44[c]		313.72 ± 0.4[c]
			75.8[d]		313.9[d]
128	SiH_2Cl_2(C_{2v}, $^1A_1$)	62.672	62.174[b]	287.486	286.734 ± 0.34[b]
			60.5[d]		286.72[c]
					285.7[d]
130	$SiHCl$(C_s, $^1A'$)	41.083	41.015[e]	251.743	251.329[e]
134	SiH($C_{\infty v}$, $^2\Pi$)	29.906	30.088[b]	198.142	198.040 ± 0.21[b]
			30.05[c]		198.05[c]
			30.054[e]		198.052[e]
135	SiH_2(C_{2v}, $^1A_1$)	34.822	34.97[c]	207.605	207.48[c]
			34.972[e]		207.481[e]
137	SiH_3(C_{3v}, $^2A_1$)	40.444	40.43[c]	217.210	216.85[c]
			40.428[e]		216.854[e]
138	SiH_4(T_d, $^1A_1$)	43.278	42.827[b]	204.917	204.653[b]
			42.79[c]		204.21[c]
			42.8[d]		204.6[d]
			42.787[e]		204.205[e]
144	Si_2H_6(D_{3d}, $^1A_{1g}$)	80.239	80.8[d]	273.329	272.7[d]
145	$SiCl$($C_{\infty v}$, $^2\Pi$)	34.646	35.780[b]	238.855	237.833 ± 0.21[b]
			35.78[c]		237.84[c]
			35.783[e]		237.837[e]
146	$SiCl_2$(C_{2v}, $^1A_1$)	51.411	51.248[b]	282.598	281.333 ± 0.8[b]
			51.27[c]		281.61[c]
			51.274[e]		281.613[e]
148	$SiCl_3$(C_{3v}, $^2A_1$)	71.277	70.733[b]	320.772	318.189 ± 4.2[b]
			70.562[e]		318.13[d]
					316.640[e]
149	$SiCl_4$(T_d, $^1A_1$)	90.751	90.261[b]	332.278	330.945 ± 0.21[b]
			90.40[c]		331.45[c]
			90.3[d]		330.7[d]
			90.404[e]		331.446[e]
156	Si_2($D_{\infty h}$, $^3\Sigma_g$)	36.642	34.452[b]	230.599	229.79[b]
			36.26[c]		238.0[c]
			34.4[d]		229.9[d]
			36.265[e]		238.004[e]
158	Si_3(C_{2v}, $^1A_1$)	51.002	50.958[e]	278.678	279.180[e]

[a] Numbering of the species is the same as in Fig. 1

[b] Ref. [41]; [c] Ref. [67]; [d] Ref. [68]; [e] Ref. [42]

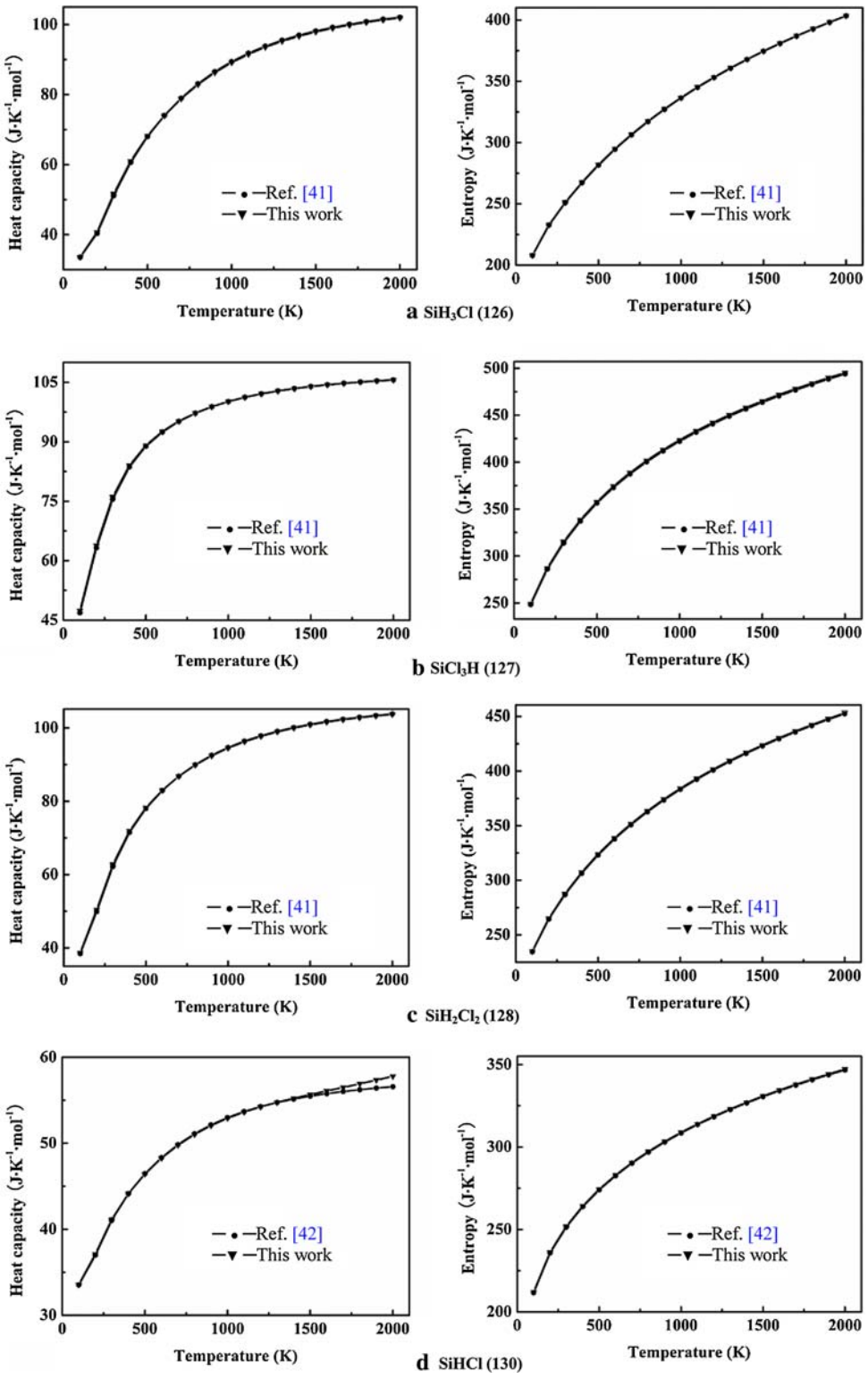

Fig. 2 Heat capacity and entropy at temperatures 100–2,000 K obtained with statistical thermodynamics and their comparisons with available experiments. Numbering of the species is the same as in Fig. 1

capacities of Si_2(156) are not consistent with both Ref. [41] and Ref. [42]. The deviation exhibits a maximum value of 4.1 J mol^{-1} K^{-1} at 500 K or 5.6 J mol^{-1} K^{-1} at 600 K compared with Ref. [41] or [42], respectively. The deviation is found mainly from the difference of electronic excitations. The electronic excitation energies in Ref. [41] should be less reliable, because they are from the 'uncertain estimates by comparison with the isoelectronic molecules C_2, BN, BeO and MgO. Reference [42] employed 15 previously obtained theoretical excitation

Fig. 2 continued

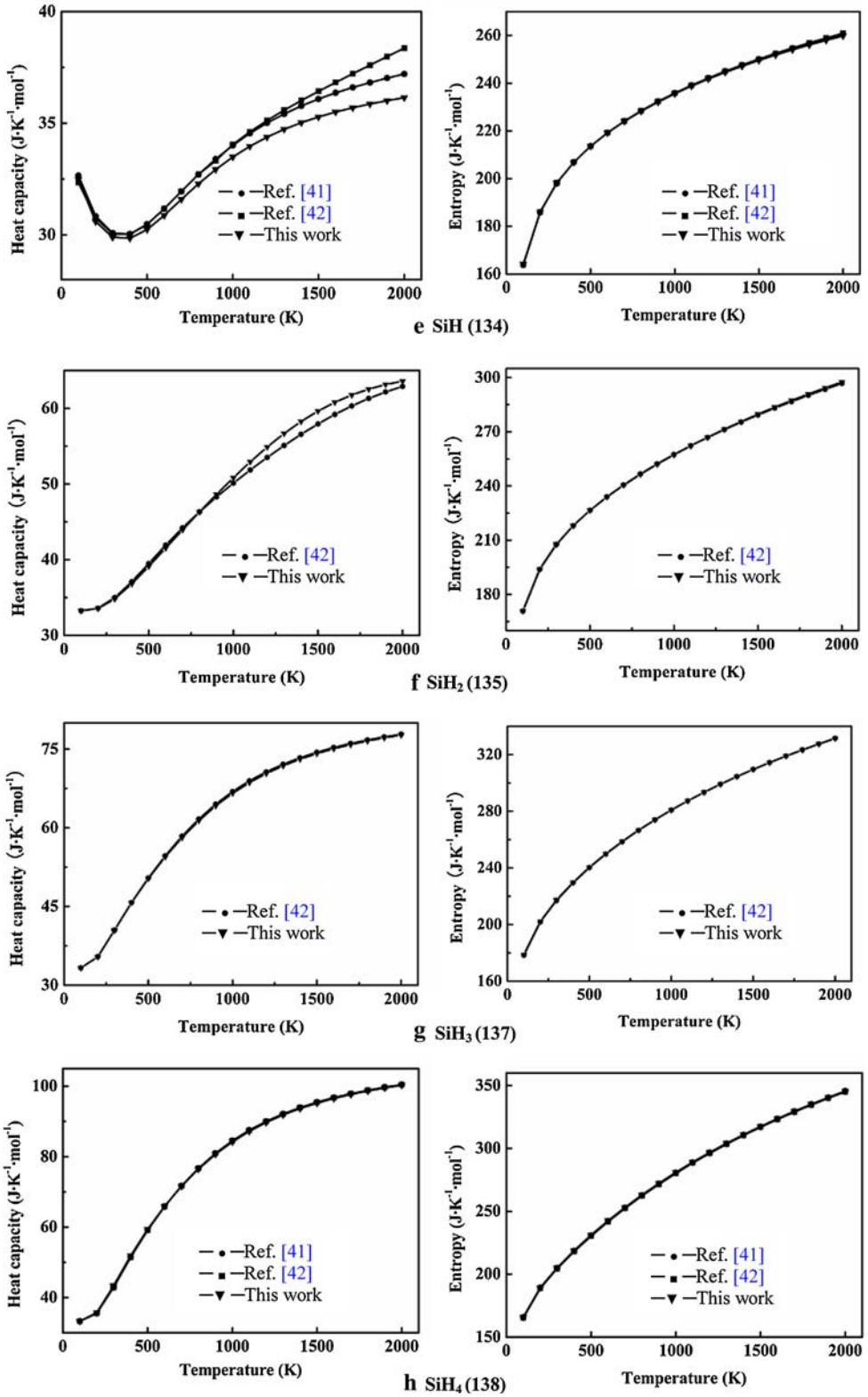

energies, among which seven are inside our truncation region of 0−1.860 eV. By examining the deviations of the heat capacities, the lowest transition energy of $X^3\Sigma_g \rightarrow A^3\Pi_u$ was found to be most significant to affect the result. Reference [42] selected 200 cm^{-1} by referring the results of 180 ± 200 cm^{-1} from the nonempirical calculation of configuration interactions [75]. However, the vertical excitation energy from TD-B3PW91/6-31G(d) is a

Fig. 2 continued

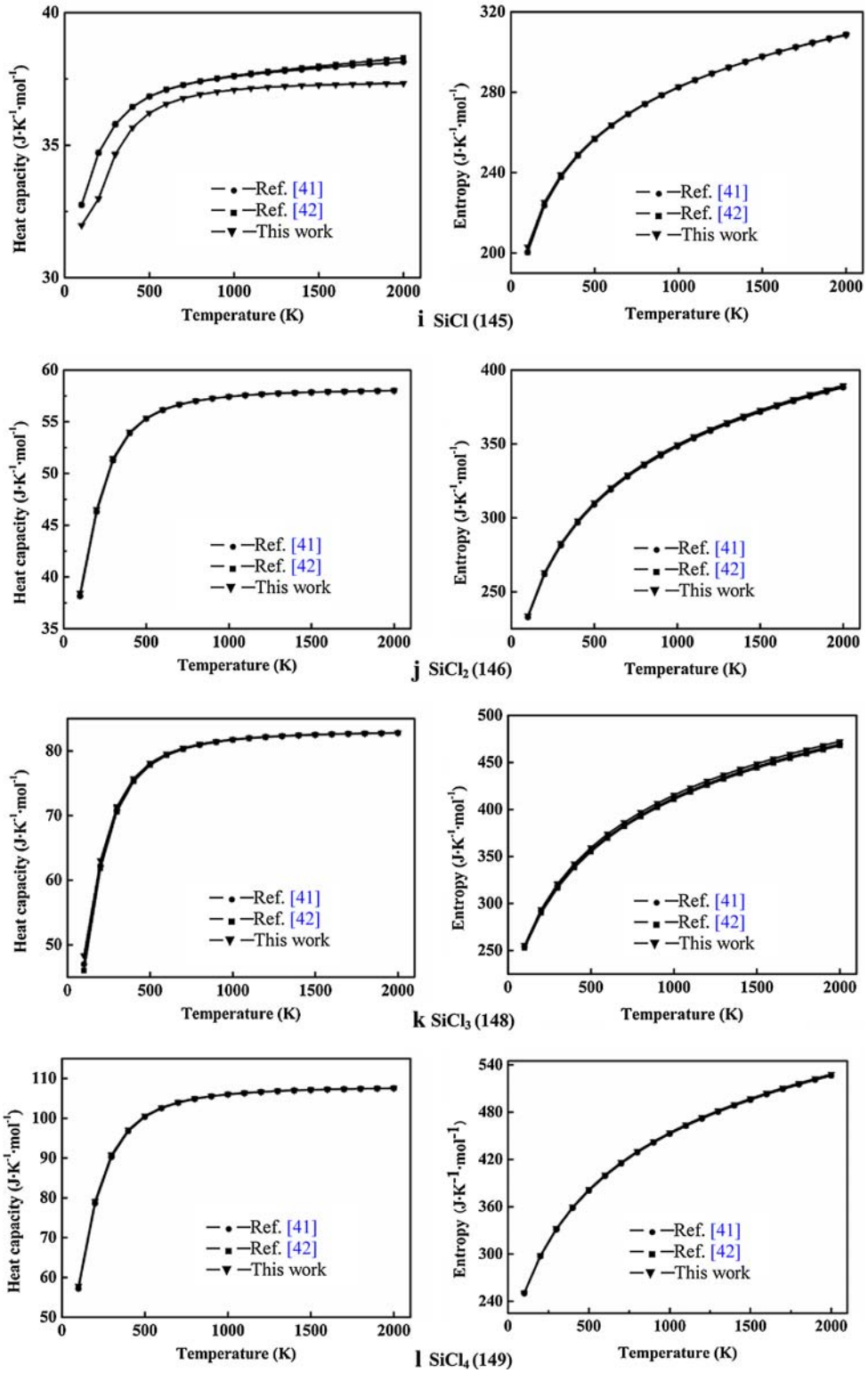

much larger value by 0.1369 eV (or 1,104 cm^{-1}). We also examined the adiabatic value with QCISD(T)/aug-cc-pvTZ and CASSCF(8,8)/6-311G(2df)-SOCISD plus Davidson corrections [76, 77] by using the GAMESS [52] plus Xi'an-CI programs [53–57]. The SOCI for the $X^3\Sigma_g$ state involves a total number of 68,052,802 configuration state functions generated from the 292 symmetry adapted CAS(8,8) reference configurations. These numbers for the

Fig. 2 continued

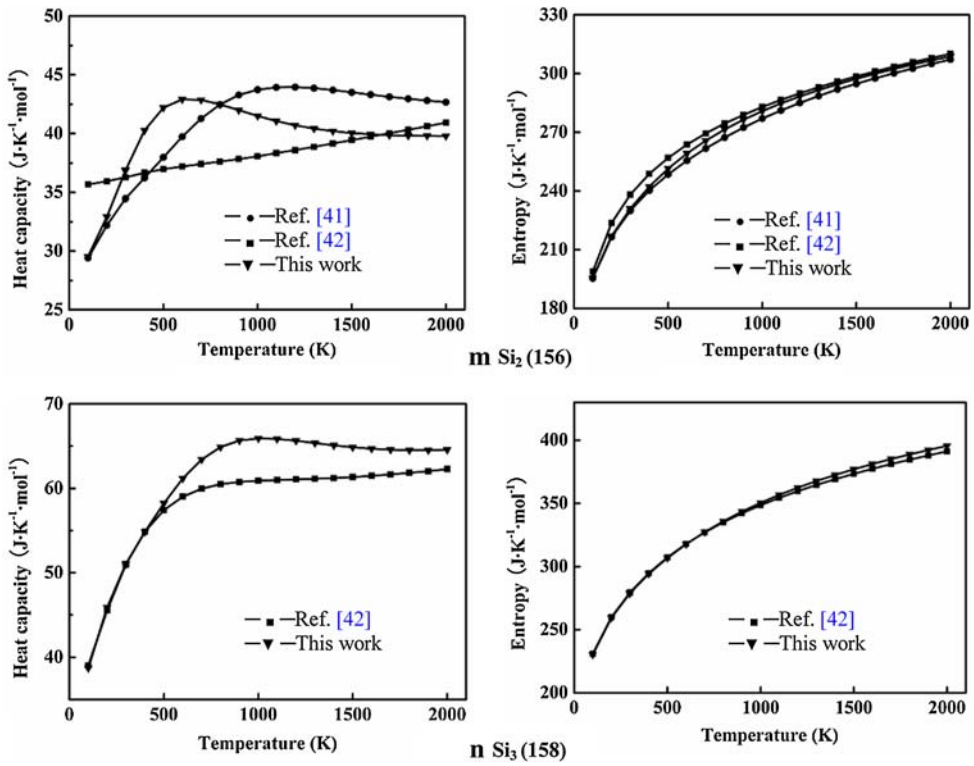

$A^3\Pi_u$ state are 69,189,358 and 296. The nondynamic electronic correlation should not be a significant problem, since the dominant state for either $X^3\Sigma_g$ or $A^3\Pi_u$ has a coefficient larger than 0.9. However, the results are even different by 0.4170 eV (or 3,363 cm^{-1}) from the QCI and 0.0394 eV (or 318 cm^{-1}) from the SOCI calculations. It is clear that the calculation of this transition is a great challenge in the development of theoretical methods. Therefore, the $X^3\Sigma_g \rightarrow A^3\Pi_u$ transition in Si_2 needs further identifications either experimentally or theoretically. The heat capacities of Si_3(158) are also consistent with the experiments within ± 1.7 J mol^{-1} K^{-1} at temperatures lower than 500 K compared with Ref. [42], but there is a maximum deviation of 5.0 J mol^{-1} K^{-1} at 1,000 K. One reason for the difference is the electronic excitation energies, where the data in Ref. [42] are for adiabatic excitations. Another is that Ref. [42] might be in error in calculating the heat capacities. This is because both Ref. [42] and the present work used the same statistical treatment, but we are not able to reproduce the results of Ref. [42] with its original data unless the degeneracy (g_i = 1) of the ground electronic state ($^1A_1$) is set at g_i = 3 (which, of course, is a mistake).

Larger deviation for entropies are found in $SiCl_3$(148) by 2.86 and 4.50 J mol^{-1} K^{-1} compared with Refs. [41] and [42], in Si_2(156) by 7.16 J mol^{-1} K^{-1} and in Si_3(158) by 4.45 J mol^{-1} K^{-1} compared with Ref. [42]. For $SiCl_3$(148), the deviation is mainly from the difference of low vibrational frequencies. For Si_2(156) and Si_3(158), the deviations are for the same reasons as discussed in the heat capacities. All of the deviations embedded in this work may also come from the deficiencies of the theoretical treatments, e.g., neglect of anharmonic effects, rigid-rotator-approximation and vertical electronic excitations. The comparison shows that the theoretical calculations of heat capacities and entropies in this work are qualified for the predictions of the other species.

To simplify the application of the high-temperature thermodynamic data, polynomial fit of the theoretical heat capacities are carried out within 298.15–2,000 K. The data have been fitted into Eq. 5 and the results are listed in Supplement Material 3. As shown in Supplement Material 3, all of the correlation coefficients are larger than 0.999 exceptions only for Si_2(156) and Si_3(158) molecules, which are larger than 0.993. Since the correlation coefficients have shown that the fit is very accurate, this paper will not list the calculated values. The results of the fitted heat capacities will be used in the high-temperature entropy, enthalpy and Gibbs free energy evaluations with classical thermodynamics.

3.3 Standard enthalpy of formation and standard Gibbs free energy of formation

The G3(MP2) and G3//B3LYP energy (U_0), the thermal correction to enthalpy (H_{corr}) and to Gibbs free energy (G_{corr})

Table 3 The experimental data of $\Delta_f H_m^\theta$(0 K), $\Delta_f H_m^\theta$(298.15 K) and $\Delta_f G_m^\theta$(298.15 K) of the gaseous Si, C, H and Cl atoms

Atom	$\Delta_f H_m^\theta$(0 K) (kJ mol^{-1})	$\Delta_f H_m^\theta$(298.15 K) (kJ mol^{-1})	$\Delta_f G_m^\theta$(298.15 K) (kJ mol^{-1})
Si	446 ± 8[a]	450 ± 8[a,b]	405.528[a]
C	711.19 ± 0.46[a]	716.67 ± 0.46[a]	671.244[a]
		716.68 ± 0.45[b]	
H	216.035 ± 0.006[a]	217.999 ± 0.006[a]	203.278[a]
		17.998 ± 0.006[a]	
Cl	119.621 ± 0.006[a]	121.302 ± 0.008[a]	105.306[a]
		121.301 ± 0.008[b]	

[a] Ref. [41]; [b] Ref. [67]

at 298.15 K are listed in Supplement Material 4. The energies and thermal corrections for C, Si, H and Cl atoms are referred to our previous work [45–47]. The standard enthalpies of formation $\Delta_f H_m^\theta$(0 K), $\Delta_f H_m^\theta$(298.15 K) and the standard Gibbs free energies of formation $\Delta_f G_m^\theta$(298.15 K) of the species are predicted according to Eqs. 6–8.

As shown in Eqs. 7 and 8, the prediction of $\Delta_f H_m^\theta$(0 K), $\Delta_f H_m^\theta$(298.15 K) and $\Delta_f G_m^\theta$(298.15 K) needs to combine the experimental data of the gaseous Si, C, H and Cl atoms. Those from Refs. [41, 67] are listed in Table 3. It is shown that the values from both the resources are almost identical. By using those from Ref. [41], the results predicted in this work are listed in Table 4 and in Supplement Material 5. Those listed in Table 4 are the experimentally available [41, 42, 67–69, 78–81] (and some of them are theoretically [82–84] available as well) species [i.e., CH_3SiCl_3(No. 1), $SiCl_2HCH_3$(7), SiH_3CH_3(107), SiH_3Cl(126), $SiCl_3H$(127), SiH_2Cl_2(128), SiHCl(130), SiH(134), SiH_2(135), SiH_3(137), SiH_4(138), Si_2H_6(144), SiCl(145), $SiCl_2$(146), $SiCl_3$(148), $SiCl_4$(149), Si_2(156) and Si_3(158)].

As shown in Table 4, the results obtained with G3(MP2) and G3//B3LYP are consistent within ±10 kJ mol^{-1} with three exceptions. These are $SiCl_2$(146) by 10.1, $SiCl_3$(148) by 14.3 and $SiCl_4$(149) by 12.9 kJ mol^{-1}. The difference is reasonable since the theoretical methods are different. By a detailed analysis, we may find that a larger portion of the deviation is from the different empirical high-level correction (HLC) in different methods (i.e., in predicting the enthalpies of formation with the atomization reactions, the deviations between the HLCs of G3(MP2) and G3//B3LYP are 4.6, 5.6 and 6.6 kJ mol^{-1} for $SiCl_2$, $SiCl_3$ and $SiCl_4$, respectively).

Table 4 Comparison of the $\Delta_f H_m^\theta$(0 K), $\Delta_f H_m^\theta$(298.15 K) and $\Delta_f G_m^\theta$(298.15 K) of the experimental or theoretical available species

No.[a]	Species (symmetry, state)	$\Delta_f H_m^\theta$(0 K) (kJ mol^{-1})		$\Delta_f H_m^\theta$(298.15 K) (kJ mol^{-1})		$\Delta_f G_m^\theta$(298.15 K) (kJ mol^{-1})	
		Cal.	Ref.	Cal.	Ref.	Cal.	Ref.
1	CH_3–$SiCl_3$(C_{3v}, $^1A_1$)	−567.8[b]		−578.0[b]	−528.858[d,e]	−514.3[b]	−468.020[d]
		−557.9[c]		−568.0[c]	−528.86[f]	−504.4[c]	−409.557[e]
					−549[g]		−490.13[h]
7	$SiCl_2H$–CH_3(C_s, $^1A'$)	−381.6[b]		−394.0[b]	−402 ± 8[g]	−339.2[b]	
		−375.0[c]		−387.4[c]		−332.6[c]	
107	SiH_3–CH_3(C_{3v}, $^1A_1$)	−12.3[b]		−27.8[b]	−29 ± 4 [g]	20.0[b]	
		−11.8[c]		−27.3[c]		20.5[c]	
126	SiH_3Cl(C_{3v}, $^1A_1$)	−129.2[b]	−132.77 ± 8[d]	−137.7[b]	−141.84 ± 8[d]	−114.3[b]	−119.292[d]
		−126.2[c]		−134.7[c]	−141.84[f]	−111.3[c]	
127	$SiCl_3H$(C_{3v}, $^1A_1$)	−489.1[b]	−491.15 ± 4.2[d]	−494.4[b]	−496.22 ± 4.2[d]	−460.8[b]	−464.899[d]
		−479.4[c]		−484.8[c]	−496.22[f]	−451.2[c]	−482.0[i]
					−482 [g]		
					−513.0[i]		
128	SiH_2Cl_2(C_{2v}, $^1A_1$)	−307.7[b]	−313.01 ± 12.6[d]	−315.1[b]	−320.49[d]	−287.9[b]	−294.900[d]
		−301.5[c]		−308.8[c]	−320.49[f]	−281.6[c]	
					−335[g]		
130	SiHCl(C_s, $^1A'$)	52.3[b]	56.322[j]	51.4[b]	54.945[j]	35.6[b]	
		57.5[c]		56.6[c]		40.8[c]	
134	SiH($C_{\infty v}$, $^2\Pi$)	361.5[b]	374.89 ± 8.4[d]	364.1[b]	376.66 ± 8.4[d]	323.7[b]	342.708[d]
		363.4[c]	374.9 ± 8.4 [g]	366.1[c]	368.64[f]	325.7[c]	
			366.942[j]		376.7 ± 8.4[g]		
					361.0[i]		
					368.636[j]		

Table 4 continued

No.[a]	Species (symmetry, state)	$\Delta_f H_m^\theta$(0 K) (kJ mol^{-1})		$\Delta_f H_m^\theta$(298.15 K) (kJ mol^{-1})		$\Delta_f G_m^\theta$(298.15 K) (kJ mol^{-1})	
		Cal.	Ref.	Cal.	Ref.	Cal.	Ref.
135	$SiH_2(C_{2v}, {}^1A_1)$	264.3[b]	275.000[j]	263.5[b]	273.33[f]	246.3[b]	
		265.2[c]		264.4[c]	289 ± 8[g]	247.2[c]	
					273.333[j]		
137	$SiH_3(C_{3v}, {}^2A_1)$	197.6[b]	210.000[j]	193.0[b]	204.52[f]	192.5[b]	
		200.7[c]		196.1[c]	202.9 ± 6.3[g]	195.5[c]	
					204.520[j]		
138	$SiH_4(T_d, {}^1A_1)$	39.4[b]	43.92 ± 2.1[d]	30.7[b]	34.31 ± 2.1[d]	53.3[b]	56.827[d]
		39.3[c]	44.318[j]	30.6[c]	34.70[f]	53.2[c]	56.9[i]
					35[g]		
					34.3[i]		
					34.700[j]		
144	$Si_2H_6(D_{3d}, {}^1A_{1\ g})$	90.1[b]	96[g]	75.8[b]	79.70 ± 1.3[f]	122.7[b]	127.7[i]
		88.9[c]		74.5[c]	80[g]	121.4[c]	
					80.3[i]		
145	$SiCl(C_{\infty v}, {}^2\Pi)$	137.9[b]	196.25 ± 6.7[d]	140.2[b]	198.32 ± 6.7[d]	108.9[b]	166.278[d]
		143.9[c]	140.287[j]	146.3[c]	189.8[i]	114.9[c]	
					142.363[j]		
					154.0 ± 8.4[k]		
					184 ± 25[l]		
					140.1[m]		
					145.1[n]		
146	$SiCl_2(C_{2v}, {}^1A_1)$	−176.3[b]	−168.74 ± 3.3[d]	−176.1[b]	−168.62 ± 3.3[d]	−186.4[b]	−180.373[d]
		−166.2[c]	−163.200[j]	−166.0[c]	−163.07[f]	−176.3[c]	
					−166 [g]		
					−163.069[j]		
148	$SiCl_3(C_{3v}, {}^2A_1)$	−327.3[b]	−398.25 ± 16.7[d]	−328.5[b]	−390.37 ± 16.7[d]	−316.1[b]	−379.858[d]
		−313.0[c]	−335.000[j]	−314.2[c]	−390.37[f]	−301.9[c]	
					−336.272[j]		
					−326 ± 13[o]		
149	$SiCl_4(T_d, {}^1A_1)$	−665.7[b]	−660.57 ± 1.3[d]	−668.5[b]	−662.75 ± 1.3[d]	−625.5[b]	−622.784[d]
		−652.8[c]	−660.076[j]	−655.6[c]	−662.20[f]	−612.6[c]	−617.0[j]
					−610 [g]		
					−657.0[i]		
					−662.200[j]		
156	$Si_2(D_{\infty h}, {}^3\Sigma_g)$	572.3[b]	587.1 ± 13[d]	577.1[b]	589.9 ± 13[d]	519.8[b]	532.653[d]
		574.1[c]	587.1 ± 13[g]	578.8[c]	583.86[f]	521.6[c]	536.0[i]
			580.000[j]		589.9 ± 13[g]		
					594.0[i]		
					583.862[j]		
158	$Si_3(C_{2v}, {}^1A_1)$	610.8[b]	625.000[j]	616.3[b]	627.869[j]	550.5[b]	
		613.5[c]		619.0[c]		553.2[c]	

[a] Numbering of the species is the same as in Fig. 1

[b] The results are from G3(MP2)

[c] The results are from G3//B3LYP

[d] Ref. [41]; [e] Ref. [78]; [f] Ref. [67]; [g] Ref. [69]; [h] Ref. [82]; [i] Ref. [68]; [j] Ref. [42]; [k] Ref. [79]; [l] Ref. [80]; [m] Ref. [83] from G3MP2B3; [n] Ref. [84] from CCSD(T)-CBS(W1U); [o] Ref. [81]

For $\Delta_f H^\theta_m$(0 K), most of the results are in excellent agreement with the experiments in Ref. [41] within ±10 kJ mol^{-1}. Larger deviations are found in SiH(134), SiCl(145), $SiCl_3$(148) and Si_2(156) by −13.4, −58.4, 71.0 and −14.8 kJ mol^{-1} from G3(MP2) and by −13.0, −52.3, 85.3 and −11.5 kJ mol^{-1} from G3//B3LYP, respectively. However, the results of $\Delta_f H^\theta_m$(0 K) for SiH(134), SiCl(145) and Si_2(156) are more close to the experiments in Ref. [42] by errors of only −5.4, −2.4, 7.7 and −7.7 kJ mol^{-1} from G3(MP2) and −3.5, 3.6, 22 and −5.9 kJ mol^{-1} from G3//B3LYP, respectively. The only larger deviation, 22 kJ mol^{-1}, shown in $SiCl_3$(148) with G3//B3LYP calculations might be from the theoretical deficiencies or the experimental value needs to be further refined. Compared with Ref. [42], the average absolute deviation is 6.3 kJ mol^{-1} from G3(MP2) and 5.9 kJ mol^{-1} from G3//B3LYP for all of the species listed in Table 4.

For the species, CH_3SiCl_3(1), $SiHCl_2CH_3$(7) and SiH_3CH_3(107), in which the experimental $\Delta_f H^\theta_m$(298.15 K) is available but $\Delta_f H^\theta_m$(0 K) is not, the theoretical $\Delta_f H^\theta_m$(298.15 K) of $SiCl_2HCH_3$(7) and SiH_3CH_3(107) are in good agreement with the values in Ref. [69], with errors of 8.0 [G3(MP2)] or 14.6 [G3//B3LYP] and 1.2 [G3(MP2)] or 1.7 [G3//B3LYP] kJ mol^{-1}, respectively. The result for CH_3SiCl_3(1) has a larger error of −49.1 [G3(MP2)] or −39.1 kJ mol^{-1} [G3//B3LYP] compared with Refs. [41, 67, 78]. There is a smaller error of −29.0 [G3(MP2)] or −19.0 kJ mol^{-1} [G3//B3LYP] compared with Ref. [69], but the deviation is still larger than the expected theoretical error bar of about ±10 kJ mol^{-1}. The result obtained in this work is consistent with the theoretical [G3(MP2)] result of our previous work in Ref. [82] in which the authors, after a detailed analysis, suggested that the experimental $\Delta_f H^\theta_m$(298.15 K) of CH_3SiCl_3 should be remeasured.

The Gibbs free energy of formation $\Delta_f G^\theta_m$(298.15 K) are also consistent with the experiments. Larger deviations are similar to those in the $\Delta_f H^\theta_m$ values and are mainly due to the errors of $\Delta_f H^\theta_m$.

It is reasonable that the theoretical calculations of $\Delta_f H^\theta_m(T)$ and $\Delta_f G^\theta_m(T)$ from the higher level G3B//B3LYP are expected to be more reliable [but those from G3(MP2) need smaller computational resources and are practical for larger molecules]. The results from G3//B3LYP for the experimentally unavailable species are listed in Supplement Material 5.

3.4 Gas-phase equilibrium diagrams

By using the thermochemical data predicted in this work, the data of 58 gas-phase species from Refs. [44−47] (where the unpublished enthalpies of fromation from G3//B3LYP for the gaseous Si_mC_n ($3 \le m+n \le 6$) clusters [46] are listed in Supplement Material 6) and 5 condensed-phase species [Si(l), Si(s), C(graphite), α-SiC and β-SiC] from Ref. [41], the equilibrium concentration distribution of the 226 species are calculated according to Eq. 11 with the code [70] developed in our group (the correctness has been confirmed compared with examples of the FactSage [85]). The results are shown in Fig. 3, where the conditions are close to the typical experiments of the CVD process in our group [86, 87] (i.e., total pressure at 6 kPa and the ratio of the input gas of CH_3SiCl_3:H_2:Ar = 1.4:4:2).

The curves plotted in Fig. 3 are for the species that have the maximum concentration (denoted by moles in a specific volume) higher than 1×10^{-7} moles in the temperature region of 300–2,000 K. Figure 3a is the overview of the equilibrium concentration distribution. Figure 3b–d is the distribution of the species having the maximum concentration in different regions (i.e., 10^{-1}−6 in Fig. 3b, 10^{-5}−10^{-1} in Fig. 3c and 10^{-7}−10^{-5} moles in Fig. 3d). It is clearly seen in Fig. 3a that the concentration for a number of species changes significantly with the formation of solid graphite at 660 K.

The concentration of the precursor MTS keeps at about 10^{-3} moles below 660 K and decreases with increasing temperature. Referring the input amount of 1.4 moles, the much lower concentration represents that MTS is a highly reactive species and is prone to decomposing especially at higher temperatures.

The amount of H_2 and HCl gases begins to increase rapidly at 660 K accompanied with the formation of condensed β-SiC and carbon (graphite). Consequently, $SiCl_4$ and CH_4 (as one of the C- and Si-bearing species) have very high concentration at temperatures below 660 K but are gradually consumed at higher temperatures. At temperatures above 1,440 K, $SiCl_2$ (another Si-bearing species) has higher concentration than $SiCl_4$, which becomes the most abundant gaseous Si-bearing species. Similarly, C_2H_2 has higher concentration than CH_4 and becomes the most abundant gaseous C-bearing species at temperatures above 1,590 K.

Most of the results are consistent with the qualitative analyses of Refs. [8, 9, 11, 17, 18, 20]. For examples, MTS, HCl, $SiCl_4$, CH_4, $SiCl_2$ and C_2H_2 have been observed [8, 9, 11, 17, 18], and $SiCl_4$ and CH_4 have higher concentration but the concentration decreases with increasing temperature [20]. There are two major differences. Reference [17] showed that the Si-bearing species $SiCl_3$ was also a dominant gaseous species at temperature in 1,000–2,200 K but it is not in the present work. The main reason is that Ref. [17] employed too low a Gibbs free energy of formation (about 78.0 kJ mol^{-1} as discussed previously in Sect. 3.3). Reference [18] showed that the C-bearing species CH_4 had the highest concentration over a wide temperature range (about 700–

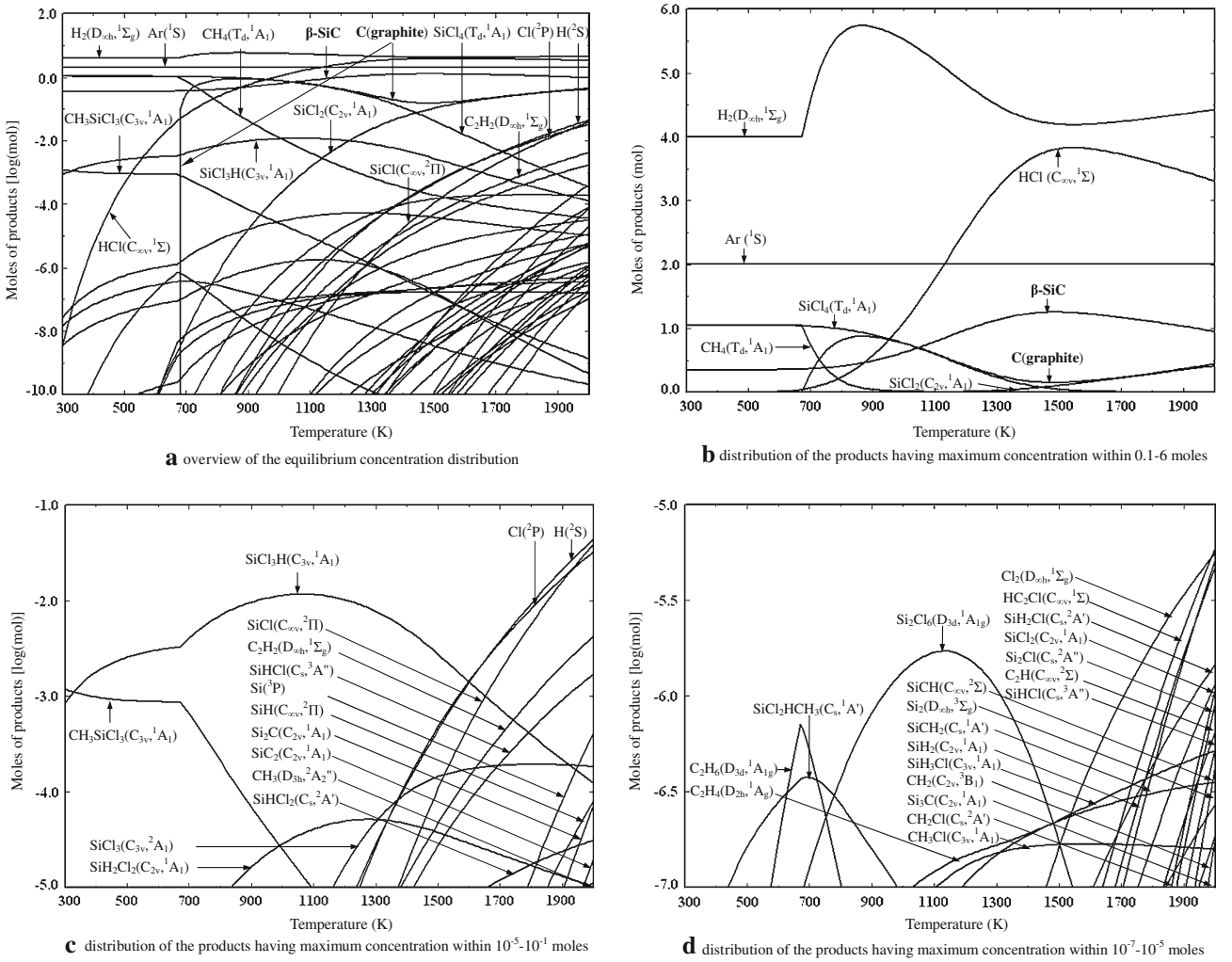

a overview of the equilibrium concentration distribution

b distribution of the products having maximum concentration within 0.1-6 moles

c distribution of the products having maximum concentration within 10^{-5}-10^{-1} moles

d distribution of the products having maximum concentration within 10^{-7}-10^{-5} moles

Fig. 3 Equilibrium concentration distribution of the 226 (221 gases, one liquid and four solids) species involved in the process of CVD preparation of silicon carbides with CH_3SiCl_3:H_2:Ar = 1.4:4:2 precursors at 6 kPa and at 300–2,000 K (only the species having a maximum concentration larger than 10^{-7} mol are shown)

1,480 K) and C_2H became the predomiant species at higher temperatures (about 1,480–1,700 K). However, this work shows that the latter C_2H radical has very low concentration (lower than 10^{-6} moles) but C_2H_2 has higher concentration at higher temperatures. The main reason is that the Gibbs free energy of formation of C_2H radical should be about 80 kJ mol^{-1} higher as has been found by our group in Ref. [44].

Figure 3a, b also shows that molecular H_2 and HCl are the predominant effluent gases in the system. At temperature above 660 K, the amount of H_2 reaches a maximum at 870 K but exhibits a minimum at 1,540 K. It is interesting that the amount of HCl has a maximum at the same temperature 1,540 K. This could be explained by the fact that H_2 is continuously consumed by further reactions (e.g., $SiCl_4 + H_2 \rightarrow SiCl_2 + 2HCl$ or $SiCl_4 + H_2 \rightarrow SiCl_3H + HCl$ or $SiCl_3H \rightarrow SiCl_2 + HCl$) within 870–1,540 K.

The amount of the condensed β-SiC and carbon increases at temperature above 660 K. It is interesting that the amount of β-SiC has a maximum (about 1.25 mol) at 1,480 K and that of carbon has a minimum (about 0.15 mol) at the same temperature, predicting that 1,480 K should be an ideal deposition temperature thermodynamically (expecting single-phase β-SiC is the desired product). This is excellently consistent with the experimental depositing temperature region of 1,100–1,300°C [86, 87].

It should be noted that carbon has high amount in Fig. 3a, b, which allows thermodynamically the codeposition of silicon carbide and carbon (even though carbon is a minor product). However, the X-ray diffraction of the products [86, 87] does not show the existence of the graphite phase. This might be from the difference between the theoretical calculation and the practical CVD/CVI process (e.g., the practical CVD/CVI process is in a flowing rather than a sealed system). The problem needs to be

further explored by combining the investigations of chemical, diffusion and crystal growth kinetics theoretically and by the help of in situ qualitative and quantitative analyses of the reaction system experimentally.

We have also tried to examine the equilibrium distribution by changing the ratio of the injected reactants with the fundamental data obtained in this work. The results show that the ideal temperature and the relative amount of codeposit substances can be easily controlled. For example, the amount of C can be reduced by higher ratio of H_2 to MTS, or C will disappear ($<10^{-7}$ moles) when the ratio is higher than 100. Similarly, the codeposit of solid Si is possible ($>10^{-7}$ moles) when the ratios of H_2 to MTS is higher than 10^4. For the ratios of 10^2–10^4, the condensed-phase β-SiC is the sole possible product. This is consistent with the observation of Refs. [17, 18, 88].

Since the standard energies of formation of β-SiC are lower than those of α-SiC, α-SiC does not appear throughout the temperature range of 300–2,000 K. This is also consistent with Refs. [17, 18].

Compared with the general discussions in the previous work [8, 9, 11, 17, 18, 20], this work has shown some additional important species (e.g., $SiCl_3H$, C_2H_2, Si_2C, $SiCl_2H_2$ and SiC_2) or radicals (e.g., H, SiCl, Cl, SiHCl, Si, $SiCl_3$, SiH, $SiHCl_2$ and CH_3) that must be closely related to the mechanisms of the reactions. The exact roles of these species could be explored by further study. Nevertheless, most of these species exhibit higher concentration ($>10^{-5}$ mol) at higher temperatures (>1,170 K) as shown in Fig. 3c except for $SiCl_3H$. The concentration of $SiCl_3H$ keeps 10^{-4} moles higher at temperatures in 300–2,000 K and exhibits a maximum (about 10^{-2} moles) at about 1,070 K. This shows that $SiCl_3H$ is really a dominant Si-bearing species as presented in Refs. [8, 9, 11, 17, 18, 20].

As shown in Fig. 3c, d, there are six gaseous species (Si_2C, SiC_2, $SiCH_2$, SiCH, $SiCl_2HCH_3$ and Si_3C) that contain both carbon and silicon are able to exist with medium concentration by 10^{-7}–10^{-4} moles at higher temperatures (i.e., 10^{-5}–10^{-4} for Si_2C and SiC_2, 10^{-7}–10^{-5} for $SiCH_2$, SiCH and Si_3C above 1,700 K) except for $SiCl_2HCH_3$, which is within 10^{-7}–10^{-6} moles in 440–990 K. This implies that the C–Si-bond bearing species could participate in the competition in the deposition process especially at higher temperatures (>1,700 K).

According to the gas-phase equilibrium diagrams (Fig. 3), strategies that could be relative to the production of the major species (i.e., CH_3SiCl_3, H_2, HCl, CH_4, $SiCl_4$, $SiHCl_3$, $SiCl_2$, C_2H_2, $SiCl_2H_2$, SiCl, SiHCl and $SiHCl_2$) can be predicted. $CH_3SiCl_3 \rightarrow CH_3 + SiCl_3$ dissociation should be a much more favorable initial decomposition reaction compared with $CH_3SiCl_3 \rightarrow CH_2SiCl_2 + HCl$, since the concentration for any of the C–Si-bond-bearing species is very low as discussed in the last paragraph. Consequently, the highly reactive radicals CH_3 and $SiCl_3$ are easy to conduct further reactions and to form the highly concentrated stable molecules CH_4, $SiCl_4$ and $SiHCl_3$. Thus, $SiCl_3 \rightarrow SiCl_2 + Cl$ and $SiHCl_3 \rightarrow SiCl_2 + HCl$ could be the major sources in the production of $SiCl_2$ above 1,440 K. Since these reactions do not produce molecular H_2, the concentration increase of H_2 could be mainly from the consecutive reactions of CH_3 (e.g., $2CH_3 \rightarrow 2C + 2H_2$) or $CH_4 \rightarrow C+2H_2$. This is also the reason for why the amount of both H_2 and C increases significantly while that of CH_4 decreases at about 660 K as discussed previously. The production of the additional important species or radicals ($SiCl_2H_2$, SiCl, SiHCl and $SiHCl_2$) could be from the reactions of $SiCl_2 + H_2 \rightarrow SiCl_2H_2$, $SiCl_2 + H_2 \rightarrow SiHCl + HCl \rightarrow SiH_2Cl_2$ and $SiCl_2 \rightarrow SiCl + Cl$ at high temperatures. The highly concentrated $SiHCl_3$ may also break its Si–H or Si–Cl bond(s) to produce SiHCl, $SiCl_2$, $SiHCl_2$ and $SiCl_3$ species.

It should be noted that the mechanism of the gas-phase chemistry in MTS-H_2 CVD/CVI system cannot be proposed only with thermodynamics. This is because that all of the analyses of the results in this work are based on the hypothesis that the system is completely in equilibrium in the point of view of thermodynamics. Additionally, the possible associated larger hydrocarbons or even the polycyclic aromatics are not considered in this work. Therefore, the detailed mechanisms of the CVD process in the preparation of silicon carbides still need further investigations.

4 Conclusions

A relatively complete set of 226 species [221 gas-phase species, 5 condensed-phase species Si(l), Si(s), C(graphite), α-SiC(s) and β-SiC(s)] that might be involved in the CVD preparation of silicon carbide in the MTS-H_2 system were considered to examine the equilibrium concentration distribution of the species thermodynamically. The structures and the thermochemical data for 163 species (among the 226) were determined theoretically. The heat capacities and entropies were evaluated with the standard statistical thermodynamics by using the structures and vibrational frequencies from B3PW91/6-31G(d) calculations and the electronic excitation energies from TD-DFT at B3PW91/6-31G(d) level or from SOCI. Accurate model chemistry G3(MP2) and G3//B3LYP theories were employed to develop the accurate energies of the species in the MTS-H_2 system.

Compared with the experimentally available species, the theoretical heat capacities, entropies, enthalpies of

formation and Gibbs free energies of formation were in agreement with those of the experiments. Most of the deviations were in excellent agreement within ± 1.7 J mol^{-1} K^{-1} for heat capacities and within ± 1.6 J mol^{-1} K^{-1} for entropies. For a few molecules (i.e., $SiCl_3$, Si_2 and Si_3), the experiments were assessed to be less reliable due to the difference of low vibrational frequencies ($SiCl_3$) or the difference of electronic excitation energies (Si_2 and Si_3). The predicted heat capacities were fitted into analytical equations within 298.15–2,000 K with correlation coefficients generally larger than 0.999. Most of the enthalpies of formation and Gibbs free energies of formation were in excellent agreement with the experiments within ± 10 kJ mol^{-1}. Some data in CH_3SiCl_3, SiH, SiCl, $SiCl_3$ and Si_2 were inconsistent with one source but were consistent with others. Comparison shows that the thermodynamics data obtained theoretically in this work were qualified for applications in the equilibrium concentration distribution calculations.

The equilibrium concentration distribution determined by using the fundamental data developed in this work and by employing the chemical equilibrium principle in the MTS-H_2 system shows that MTS is a highly reactive species and is prone to decomposing especially at higher temperatures. $SiCl_4$ and CH_4 (one of the C- and Si-bearing species) have very high concentration at temperatures below 660 K and are gradually consumed at higher temperatures. At temperatures above 1,440 K, $SiCl_2$ (another Si-bearing species) becomes the most abundant gaseous Si-bearing species. At temperatures above 1,590 K, C_2H_2 becomes the most abundant gaseous C-bearing species. Molecular H_2 and HCl are the predominant effluent gases. At temperature above 660 K, the amount of H_2 reached a maximum at 870 K and exhibited a minimum at 1,540 K. The amount of HCl has a maximum at 1,540 K. The amount of the condensed β-SiC and carbon increases at temperature above 660 K. The amount of β-SiC has a maximum (about 1.25 mol) at 1,480 K and that of carbon has a minimum (about 0.15 mol) at the same temperature, predicting that 1,480 K is an ideal deposition temperature thermodynamically (assuming that single-phase β-SiC is the desired product).

This work has provided more fundamental data for analyzing the thermochemisty of the CVD process of the MTS-H_2 system at any ratio of the input precursors to control the formation of the solid β-SiC, C and Si.

Acknowledgments Part of the calculations was performed in the High Performance Computing Center of the Northwestern Polytechnical University. Supports by the National Natural Science Foundation of China (No. 50572089, No. 50642039) and the Chinese 973 Fundamental Research are greatly acknowledged.

References

1. Fitzer E, Kehr D (1976) Carbon, carbide and silicide coatings. Thin Solid Films 39:55–57. doi:10.1016/0040-6090(76)90623-4
2. Powell JA, Matus LG (1989) In: Harris GL, Yang CY-W (eds) Amorphous and crystalline silicon carbide (Springer proceedings in physics, vol 34). Springer, Berlin, p 2
3. Buljan ST, Pesto AE, Kim HJ (1989) Ceramics whiskers and particulate composites: properties, reliability and applications. Am Ceram Soc Bull 68:387–394
4. Loumagne F, Langlais F, Naslain R (1995) Experimental kinetic study of the chemical vapour deposition of SiC-based ceramics from CH_3SiCl_3/H_2 gas precursor. J Cryst Growth 155:198–204. doi:10.1016/0022-0248(95)00180-8
5. Loumagne F, Langlais F, Naslain R et al (1995) Physicochemical properties of SiC-based ceramics deposited by low pressure chemical vapor deposition from CH_3SiCl_3/H_2. Thin Solid Films 254:75–82. doi:10.1016/0040-6090(94)06237-F
6. Loumagne F, Langlais F, Naslain R (1995) Reactional mechanisms of the chemical vapour deposition of SiC-based ceramics from CH_3SiCl_3/H_2 gas precursor. J Cryst Growth 155:205–213. doi:10.1016/0022-0248(95)00181-6
7. Josiek A, Langlais F (1996) Residence-time dependent kinetics of CVD growth of SiC in the MTS/H_2 system. J Cryst Growth 160:253–260. doi:10.1016/0022-0248(95)00744-X
8. Jonas S, Ptak WS, Sadowski W et al (1995) FTIR in situ studies of the gas phase reactions in chemical vapor deposition of SiC. J Electrochem Soc 142:2357–2362. doi:10.1149/1.2044300
9. Hopfe V, Mosebach H, Erhard M et al (1995) In-situ FTIR emission spectroscopy in a technological environment: chemical vapour infiltration (CVI) of SiC composites. J Mol Struct 347:331–342. doi:10.1016/0022-2860(95)08555-A
10. Papasouliotis GD, Sotirchos SV (1995) Gravimetric investigation of the deposition of SiC films through decomposition of methyltrichlorosilane. J Electrochem Soc 142:3834–3844. doi:10.1149/1.2048421
11. Ganz M, Dorval N, Lefebvre M et al (1996) In situ optical analysis of the gas phase during the deposition of silicon carbide from methyltrichiorosilane. J Electrochem Soc 143:1654–1661
12. Papasouliotis GD, Sotirchos SV (1998) Hydrogen chloride effects on the CVD of silicon carbide from methyltrichlorosilane. Chem Vap Depos 4:235–246 doi:10.1002/(SICI)1521-3862(199812)04:06<235::AID-CVDE235>3.0.CO;2-R
13. Hüttinger KJ (1998) CVD in HotWall reactors—the interaction between homogeneous gas-phase and heterogeneous surface reactions. Chem Vap Depos 4:151–158 doi:10.1002/(SICI)1521-3862(199807)04:04<151::AID-CVDE151>3.0.CO;2-2
14. Papasouliotisa GD, Sotirchos SV (1998) Steady-state multiplicity phenomena in the deposition of silicon carbide. J Electrochem Soc 145:3908–3919. doi:10.1149/1.1838892
15. Papasouliotisa GD, Sotirchos SV (1999) Experimental study of atmospheric pressure chemical vapor deposition of silicon carbide from methyltrichlorosilane. J Mater Res 14:3397–3409. doi:10.1557/JMR.1999.0460
16. Sone H, Kaneko T, Miyakawa N (2000) In situ measurements and growth kinetics of silicon carbide chemical vapor deposition from methyltrichlorosilane. J Cryst Growth 219:245–252. doi:10.1016/S0022-0248(00)00616-3
17. Willian BP (1993) Chemical vapor deposition of silicon carbide in the methyltrichlorosilane–hydrogen system. PhD thesis, The Ohio State University
18. Boisvert RP (1995) A thermodynamic and kinetic study of the deposition of SiC from various precursor systems with application to the preparation of lamellar-matrix/continuous fiber-

reinforced composites. PhD thesis, Rensselaer Polytechnic Institute, Troy, New York
19. Zhang WG, Hüttinger KJ (2001) CVD of SiC from methyltrichlorosilane. Part II: composition of the gas phase and the deposit. Chem Vap Depos 7:173–181 doi:10.1002/1521-3862(200107)7:4<173::AID-CVDE173>3.0.CO;2-X
20. Reznik B, Gerthsen D, Zhang WG, Hüttinger KJ (2003) Microstructure of SiC deposited from methyltrichlorosilane. J Eur Ceram Soc 23:1499–1508. doi:10.1016/S0955-2219(02)00364-3
21. Allendorf MD, Kee RJ (1991) A model of silicon carbide chemical vapor deposition. J Electrochem Soc 138:841–852. doi:10.1149/1.2085688
22. Lee YL, Sanchez JM (1997) Theoretical study of thermodynamics relevant to tetramethylsilane pyrolysis. J Cryst Growth 178:513–517. doi:10.1016/S0022-0248(97)00091-2
23. Allendorf MD, Melius CF (1992) A model of silicon carbide chemical vapor deposition. J Phys Chem 96:429–437. doi:10.1021/j100180a080
24. Su MD, Schlegel HB (1993) An ab initio MO study of the thermal decomposition of chlorinated monosilanes, SiH_4–nCl_n, ($n = 0$–4). J Phys Chem 97:9981–9985. doi:10.1021/j100141a015
25. Vorob'ev AN, Karpov SY, Zhmakin AI et al (2000) Effect of gas-phase nucleation on chemical vapor deposition of silicon carbide. J Cryst Growth 211:343–346. doi:10.1016/S0022-0248(99)00776-9
26. Allendorf MD, Melius CF (1993) Theoretical study of the thermochemistry of molecules in the Si–C–Cl–H system. J Phys Chem 97:720–728. doi:10.1021/j100105a031
27. Papasouliotis GD, Sotirchos SV (1994) On the homogeneous chemistry of the thermal decomposition of methyltrichlorosilane. J Electrochem Soc 141:1599–1611. doi:10.1149/1.2054969
28. Osterheld TH, Allendorf MD, Melius CF (1994) Unimolecular decomposition of methyltrichlorosilane: RRKM calculations. J Phys Chem 98:6995–7003. doi:10.1021/j100079a018
29. Zhang WG, Hüttinger KJ (2001) CVD of SiC from methyltrichlorosilane. Part I deposition rates. Chem Vap Depos 7:167–172 doi:10.1002/1521-3862(200107)7:4<167::AID-CVDE167>3.0.CO;2-L
30. Mousavipour SH, Saheb V, Ramezani S (2004) Kinetics and mechanism of pyrolysis of methyltrichlorosilane. J Phys Chem A 108:1946–1952. doi:10.1021/jp0306592
31. Ge Y, Gordon MS, Battaglia F et al (2007) Theoretical study of the pyrolysis of methyltrichlorosilane in the gas phase. 1. Thermodynamics. J Phys Chem A 111:1462–1474. doi:10.1021/jp065453q
32. Ge Y, Gordon MS, Battaglia F et al (2007) Theoretical study of the pyrolysis of methyltrichlorosilane in the gas phase. 2. Reaction paths and transition states. J Phys Chem A 111:1475–1486. doi:10.1021/jp065455a
33. Xu YD, Cheng LF, Zhang LT et al (2001) High toughness, 3D textile, SiC/SiC composites by chemical vapor infiltration. Mater Sci Eng A 318:183–188. doi:10.1016/S0921-5093(01)01303-X
34. Nannetti CA, Riccardi B, Ortona A (2002) Development of 2D and 3D Hi-Nicalon fibres/SiC matrix composites manufactured by a combined CVI-PIP route. J Nucl Mater 307–311:1196–1199. doi:10.1016/S0022-3115(02)00956-X
35. Luthra KL (2002) Melt infiltrated (MI) SiC/SiC composites for gas turbine applications. Presented at DER peer review for microturbine and industrial gas turbines programs, Fairfax, Virginia, March 12–14, 2002
36. Brennan JJ (2000) Interfacial characterization of a slurry-cast melt-infiltrated SiC/SiC ceramic–matrix composite. Acta Mater 48:4619–4628. doi:10.1016/S1359-6454(00)00248-2
37. Yano T, Budiyanto K, Yoshida K (1998) Fabrication of silicon carbide fiber-reinforced silicon carbide composite by hot-pressing. Fusion Eng Des 41(1–4):157–163. doi:10.1016/S0920-3796(98)00094-5
38. Lee SP, Katoh Y, Kohyama A (2001) Microstructure analysis and strength evaluation of reaction sintered SiC/SiC composites. Scr Mater 44(1):153–157. doi:10.1016/S1359-6462(00)00542-X
39. Golecki I (1997) Rapid vapor-phase densification of refractory composites. Mater Sci Eng R20:37–124
40. Allendorf MD, Melius CF (1998) Understanding gas-phase reactions in the thermal CVD of hard coatings using computational methods. Surf Coat Tech 108/109:191–199. doi:10.1016/S0257-8972(98)00660-4
41. Chase MW Jr (1998) NIST-JANAF thermochemical tables, fourth edition. J Phys Chem Ref Data Monograph No. 9
42. Gurvich LV, Veyts IV, Alcock CB (1989) Thermodynamic properties of individual substances, 4th edn. Hemisphere Publishing, New York
43. National Standard Reference Data System (1982) The NBS tables of chemical thermodynamic properties. Selected values for inorganic and C1 and C2 organic substances in SI units. J Phys Chem Ref Data 11(Suppl 2)
44. Yao XP, Su KH, Deng JL et al (2007) Gas-phase reaction thermodynamics in preparation of pyrolytic carbon by propylene pyrolysis. Comput Mater Sci 40:504–524. Erratum: Deng JL, Su KH, Yao XP et al (2008) Comput Mater Sci (in press). doi:10.1016/j.commatsci.2008.05.015
45. Deng J, Su K, Zeng Y et al (2008) Investigation of thermodynamic properties of gaseous SiC($X^3\Pi$ and $a^1\Sigma$) with accurate model chemistry calculations. Physica A 387(22):5440–5456
46. Deng J, Su K, Wang X et al (2008) Thermodynamic properties of the most stable gaseous small silicon–carbon clusters in their ground states. Eur Phys J D 49:21–35
47. Zeng Y, Su KH, Deng JL et al (2008) Thermodynamic investigation of the gas-phase reactions in the chemical vapor deposition of boron carbide with BCl_3–CH_4–H_2 precursors. J Mol Struct Theochem 861(1–3):103–116. doi:10.1016/j.theochem.2008.04.016
48. Su KH, Wei J, Hu XL et al (2000) Systematic comparison of geometry optimization on inorganic molecules. Acta Phys Chim Sin 16:643–651
49. Scott AP, Radom L (1996) Harmonic vibrational frequencies: an evaluation of Hartree–Fock, Møller–Plesset, quadratic configuration, density functional theory and semiempirical scale factor. J Chem Phys 100:16502–16513. doi:10.1021/jp960976r
50. Merrick JP, Moran D, Radom L (2007) An evaluation of harmonic vibrational frequency scale factors. J Phys Chem A 111:11683–11700. doi:10.1021/jp073974n
51. Petersilka M, Gossmann UJ, Gross EKU (1996) Excitation energies from time-dependent density-functional theory. Phys Rev Lett 76:1212–1215. doi:10.1103/PhysRevLett.76.1212
52. Schmidt MW, Baldridge KK, Boatz JA et al (1993) General atomic molecular electronic structure system. J Comput Chem 14:1347–1363
53. Wang YB, Zhai GH, Suo BB et al (2003) Hole–particle correspondence in CI calculations. Chem Phys Lett 375:134–140. doi:10.1016/S0009-2614(03)00849-2
54. Wang YB, Suo BB, Zhai GH et al (2004) Doubly contracted CI method. Chem Phys Lett 389:315–320. doi:10.1016/j.cplett.2004.03.092
55. Wang YB, Han HX, Zhai GH et al (2004) Doubly contracted CI method and applications. Sci China B 47:276–282. doi:10.1360/03yb0256
56. Suo B, Zhai GH, Wang YB et al (2005) Parallelization of MRCI based on hole–particle symmetry. J Comput Chem 26:88–96. doi:10.1002/jcc.20148
57. Gan Z, Su K, Wang Y et al (1999) A method to fast determine the coupling coefficients in CI calculations. Sci China B 42:43–52
58. Curtiss LA, Redfern PC, Raghavachari K et al (1999) Gaussian-3 theory using reduced Møller–Plesset order. J Chem Phys 110:4703–4709. doi:10.1063/1.478385

59. Baboul AG, Curtiss LA, Redfern PC et al (1999) Gaussian-3 theory using density functional geometries and zero-point energies. Chem Phys 110:7650–7657. doi:10.1063/1.478676
60. Curtiss LA, Raghavachari K, Redfern PC et al (1997) nt of Gaussian-2 and density functional theories for the computation of enthalpies of formation. J Chem Phys 106:1063–1079. doi:10.1063/1.473182
61. Curtiss LA, Redfern PC, Raghavachari K et al (1998) Assessment of Gaussian-2 and density functional theories for the computation of ionization potentials and electron affinities. J Chem Phys 109:42–55. doi:10.1063/1.476538
62. Su KH, Deakyne CA (1995) Review of the Gaussian-2 theory, its applications and the prediction of the enthalpy of formation. Prog Chem 7(2):128–139
63. Curtiss LA, Raghavachari K (1995) In: Langhoff SR (ed) Quantum mechanical electronic structure calculations with chemical accuracy, vol 139. Kluwer, Dordrecht
64. Raghavachari K, Curtiss LA (1995) In: Yarkony DR (ed) Modern electronic structure theory, vol 991. World Scientific, Singapore
65. Frisch MJ, Trucks GW, Schlegel HB, Scuseria GE, Robb MA, Cheeseman JR et al (2003) Gaussian 03, Revision B.01. Gaussian Inc., Pittsburgh
66. NIST chemistry webbook. Available at http://webbook.nist.gov/chemistry/
67. Cox JD, Wagman DD, Medvedev VA (1989) CODATA key values for thermodynamics. Hemisphere Publishing, New York
68. Lide DR (ed) (1996/1997) CRC handbook of chemistry and physics, 77th edn. CRC Press, Boca Raton
69. Lias SG, Bartmess JE, Liebman JF et al (1988) Gas-phase ion and neutral thermochemistry. J Phys Chem Ref Data 17 (Suppl 1)
70. Zeng QF (2001) PhD thesis, Northwestern Polytechnical University
71. Grev RS, Schaefer HF (1985) The ground state of Si_3, two near degenerate isomers. Chem Phys Lett 119:111–118. doi:10.1016/0009-2614(85)80043-9
72. Diercksen GHF, Grüner NE, Oddershede J et al (1985) The structure of Si_2C and Si_3. Chem Phys Lett 117:29–32. doi:10.1016/0009-2614(85)80398-5
73. Balasubramanian K (1986) CAS SCF/CI calculations of low-lying states and potential energy surfaces of Si_3. Chem Phys Lett 125:400–406. doi:10.1016/0009-2614(86)85180-6
74. Slanina Z (1986) On thermodynamics of Si_3(g) isomers. Chem Phys Lett 131:420–425. doi:10.1016/0009-2614(86)87178-0
75. Lüthi HP, McLean AD (1987) Can the lowest two electronic states of Si_2 be ordered? Chem Phys Lett 135:352–356. doi:10.1016/0009-2614(87)85170-9
76. Langhoff SR, Davidson ER (1977) Int J Quantum Chem S11:149
77. Davidson ER, Feller D, McMarchie LE et al (1994) MELD. Indiana University, Bloomington
78. Chase MW, Davies JCA, Downey JR et al (1985) J Phys Chem Ref Data 14(Suppl 1)
79. Hildenbrand DL, Lau KH, Sanjuro A (2003) Experimental thermochemistry of the SiCl and SiBr radicals; enthalpies of formation of species in the Si–Cl and Si–Br systems. J Phys Chem A 107:5448–5451. doi:10.1021/jp022524m
80. Weber ME, Armentrout PB (1989) Energetics and mechanisms in the reaction of Si+ with $SiCl_4$. Thermochemistry of SiCl, $SiCl^+$, and $SiCl_2^+$. J Phys Chem 93:1596–1604. doi:10.1021/j100341a082
81. Fisher ER, Armentrout PB (1991) Reactions of O^{2+}, Ar^+, Ne^+, and He^+ with $SiCl_4$: thermochemistry of $SiCl_x^+$. J Phys Chem 95:4765–4772. doi:10.1021/j100165a032
82. Zeng QF, Su KH, Zhang LT et al (2006) Evaluation of the thermodynamic data of CH_3SiCl_3 based on quantum chemistry calculations. J Phys Chem Ref Data 35:1385–1390. doi:10.1063/1.2201867
83. Janoschek R, Rossi MJ (2004) Thermochemical properties from G3MP2B3 calculations, set-2: free radicals with special consideration of CH_2=CH–C=CH_2, cyclo-C_5H_5, CH_2OOH, HO–CO, and HCOO. Int J Chem Kinet 36:661–686. doi:10.1002/kin.20035
84. Janoschek R, Fabian WMF (2006) Enthalpies of formation of small free radicals and stable intermediates: interplay of experimental and theoretical values. J Mol Struct 780/781:80–86. doi:10.1016/j.molstruc.2005.04.050
85. FactSage 5.4.1 (2006) Montreal, Quebec, Canada
86. Xiao P, Xu YD, Huang BY (2002) Effects of deposition conditions on deposition thermodynamics and morphology of CVD-SiC. J Inorg Mater 17:877–881
87. Deng Q, Xiao P, Xiong X (2006) Effect of temperature on microstructure and composition of CVD SiC coating. Mater Sci Eng Powder Metall 11:305–309
88. Naslain R, Langlais F, Feou R (1989) The CVI-processing of ceramic matrix composites. J Phys 50:C5. 191–C5. 207
89. Jacoxa ME (2003) Vibrational and electronic energy levels of polyatomic transient molecules. J Phys Chem Ref Data Suppl B 32:1–441. doi:10.1063/1.1497629